Chapter 4

SYNTHESIS AND NLO PROPERTIES OF CHALCONE BASED COMPOUNDS

4.1 Introduction:

A series of chalcone derivatives have been synthesized, with different donor and acceptor groups to create a push-pull system in the molecule, using conventional Claisen-Schmidt reaction (Scheme 4.1). The structure resembles either $D - \pi - A - \pi - D$ or $D - \pi - A - \pi - A$ motif. In chalcone, the carbonyl group at the center acts as an acceptor of the electron. To determine how effective this acceptor part (–C=O) is to induce charge transfer & nonlinearity, the carbonyl group was substituted in some selective chalcones by reacting with (2,4-dinitrophenyl)hydrazine. A series of hydrazone derivative of chalcone was synthesized using Scheme 4.2. Hydrazones have an azomethine -NHN=CH- proton, this class is of importance for new drug development. Many researchers have synthesized these compounds as target structures and evaluated their biological activities. The main supramolecular interactions between these molecules are strong hydrogen bonds between the hydrazone and the nitro groups, which influence the molecular packing, also the nonlinear behavior. The compounds were characterized and the linear, nonlinear optical properties of both the series were measured [1, 2].

4.2 Synthesis of chalcone derivatives:

To a solution of NaOH (40% w/v) in ethanol and water, placed in an ice bath, acetophenone / acetophenone derivative (1 mmol) was added. After 15-20 min benzaldehyde/ benzaldehyde derivative (1 mmol) was mixed in it. The progress of the reaction was monitored by TLC using hexane and ethyl acetate gradient as the mobile phase. The temperature was maintained at 25˚-27˚C and stirred for an appropriate time (mentioned in Table 4.1). The reaction mixture was refrigerated overnight and neutralized with conc. HCl, the precipitate obtained was filtered, washed with water till the pH was neutral. The product was dried and purified by column chromatography using a gradient of chloroform and methanol as eluent.

Reaction condition and physical data of the chalcone derivatives are given in Table 4.1.
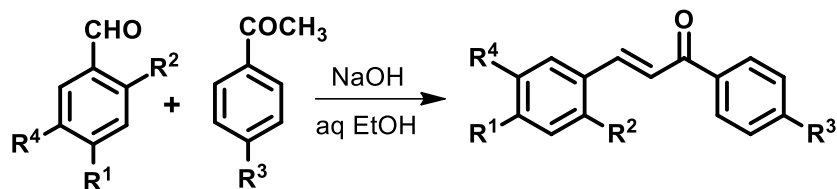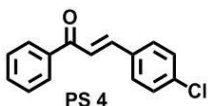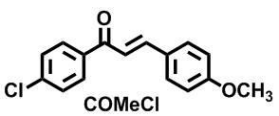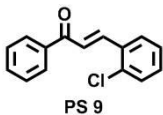

Scheme 4.1: Synthesis of chalcone derivatives.
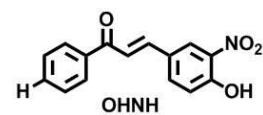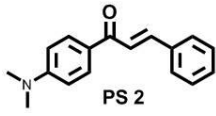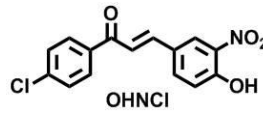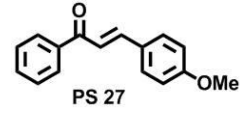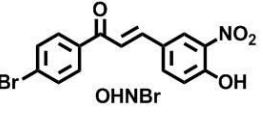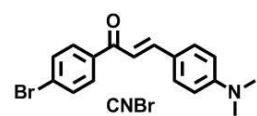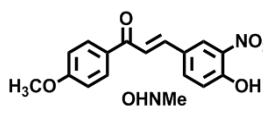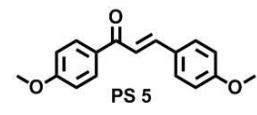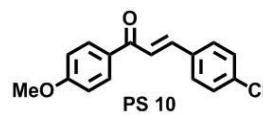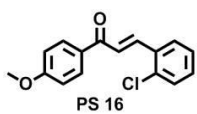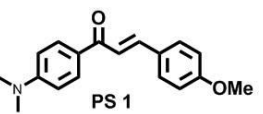
Table 4.1: Reaction condition and physical data of chalcone derivatives.

Compound & Code	Time	M.P. (℃)	Compound & Code	Time	M.P. (℃)
PS 4	15 min	60-62	COMeCl / OCH₃	15 h	119-120
PS 9	3.5 h	102-105	OHNH	4 h	121-123
PS 2	30 min	91-93	OHNCl	4 h	170-172
PS 27	2 h	109-110	OHNBr	4 h	177-179
CNBr	96 h	115-116	OHNMe	5 h	153-155
PS 5	24 h	105-106	PS 10	10 h	118-119
PS 16	10 h	117-118	PS 1	5 h	120-123

4.3 Characterization of chalcone derivatives:
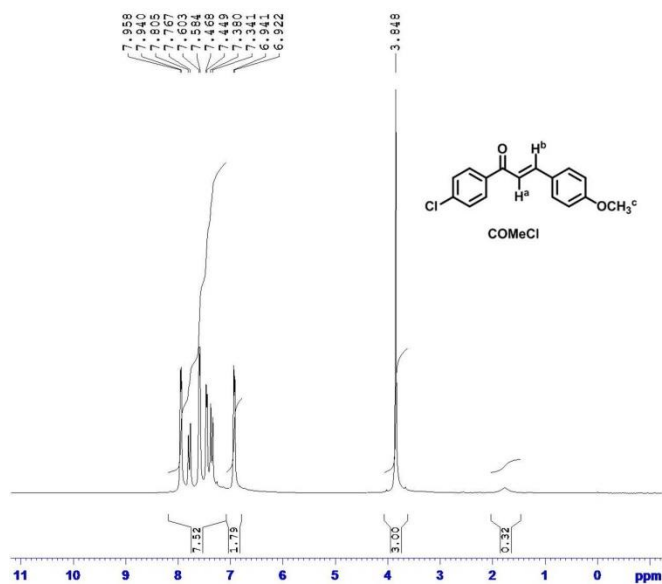
Figure 4.1: ^{1}H NMR spectrum of *(E)-1-(4-chlorophenyl)-3-(4-methoxyphenyl)prop-2-en-1-one* (**COMeCl**).
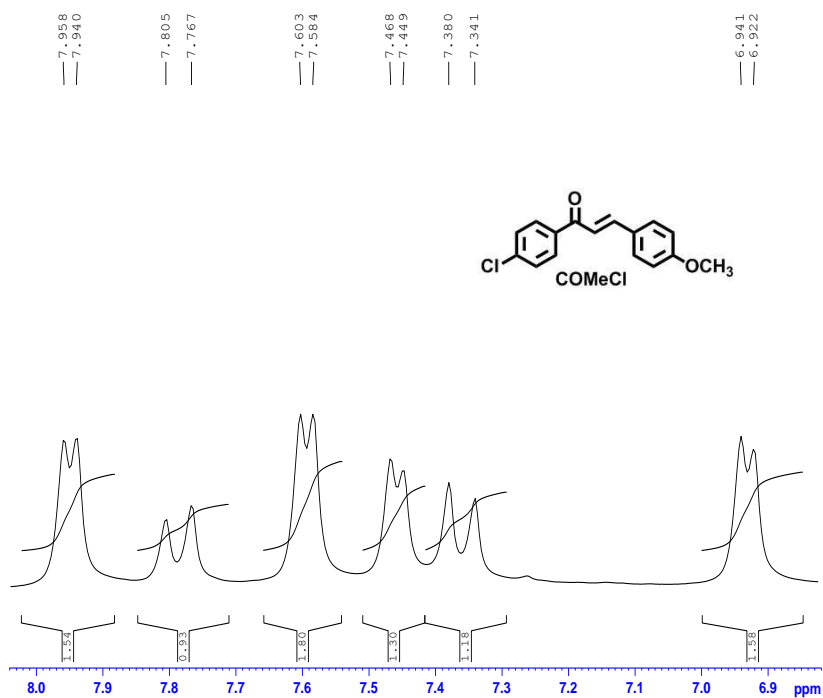
Figure 4.2: ^{1}H NMR spectrum of *(E)-1-(4-chlorophenyl)-3-(4-methoxyphenyl)prop-2-en-1-one* (**COMeCl**) showing region 6.9-8.0 ppm.

Fig. 4.1 shows the ^{1}H NMR (400 MHz, CDCl₃) spectrum of *(E)-1-(4-chlorophenyl)-3-(4-methoxyphenyl)prop-2-en-1-one* **(COMeCl)** and Fig. 4.2 shows the region around 6.9-8.0 ppm. H^a and H^b appears at 7.76 and 7.34 ppm respectively, they have a high coupling constant of 16 Hz, which is an indication of a trans-configuration of the double bond as *trans* coupling constants are generally larger than *cis*-coupling constant. H^c protons appear as a singlet at 3.83 ppm. The aromatic protons having *J* value of 8 Hz appears in the region 6.9-8.0 ppm.

The characterization data of other chalcone derivatives are presented in the following section. The spectra of other compounds in the series are available in the Section 4.16.

(E)-1-(4-bromophenyl)-3-(4-hydroxy-3-nitrophenyl)prop-2-en-1-one **(OHNBr):** **OHNBr** was synthesized following the method described in Section 4.2 with 4-bromoacetophenone (199 mg) and 4-hydroxy-3-nitrbenzaldehyde (169 mg). Synthesis of 4-hydroxy-3 nitro benzaldehyde was accomplished via nitration of 4 hydroxybenzaldehyde following the method reported by P. Ionita [3]. TLC was done using chloroform: methanol (9:1) as developing solvent. The compound was purified by silica gel column (60-120 mesh) chromatography using chloroform as eluent. Shiny yellow solid. Yield: 245 mg (70%). ^{1}H NMR (400 MHz, CDCl₃) δ 10.76 (s, 1H), 8.39 (s, 1H), 7.87-7.91 (m, 4H), 7.89-7.86 (dd, *J* = 2 Hz and *J* = 2 Hz, 1H), 7.78 (d, *J* = 15.6 Hz, 1H), 7.47 (d, *J* = 15.6 Hz, 1H), 7.23 (d, *J* = 8 Hz, 1H). ^{13}C NMR (CDCl₃) δ 188.6, 156.4, 142.1, 136.6, 136.5, 132.1, 130.0, 127.5, 121.1, 121.9, 120.9.

(E)-1-(4-chlorophenyl)-3-(4-hydroxy-3-nitrophenyl)prop-2-en-1-one (**OHNCl**): **OHNCl** was synthesized following the method described in Section 4.2 with 4-chloroacetophenone (155 mg) and 4-hydroxy-3-nitrbenzaldehyde (169 mg). TLC was done using chloroform: methanol (9:1) as developing solvent. The compound was purified by silica gel column (60-120 mesh) chromatography using chloroform as eluent. Shiny yellow solid. Yield: 199 mg (65%). ^{1}H NMR (400

MHz, CDCl$_3$) δ 10.76 (s, 1H), 8.39 (s, 1H), 7.99-7.95 (m, 4 H), 7.89-7.87 (dd, J = 2 Hz and J = 2 Hz, 1H), 7.78 (d, J = 15.6 Hz, 1H), 7.47 (d, J = 15.6 Hz, 1H), 7.23 (d, J = 8 Hz, 1H). ^{13}C (CDCl$_3$) δ 188.4, 188.3, 156.3, 142.0, 136.6, 129.9, 129.8, 129.0, 125.1, 121.9, 120.9.

(E)-3-(4-hydroxy-3-nitrophenyl)-1-(4-methoxyphenyl)prop-2-en-1-one
(OHNMe): OHNMe was synthesized following the method described in Section 4.2 with 4-methoxyacetophenone (150 mg) and 4-hydroxy-3-nitrbenzaldehyde (169 mg). TLC using chloroform: methanol (9:1) as developing solvent. The compound was purified by silica gel column (60-120 mesh) chromatography using chloroform as eluent. Occur yellow solid. Yield: 210 mg (70%). ^{1}H NMR (400 MHz, CDCl$_3$) δ 10.74 (s, 1H), 8.37 (s, 1H), 7.89-7.86 (dd, J = 2 Hz and J = 2 Hz 1H), 7.75 (d, J = 15.6 Hz, 1H), 7.47 (d, J = 15.6 Hz, 1H), 7.22 (d, J = 8 Hz, 1H), 7.01-6.98 (m, 2H), 3.09 (s, 3H). ^{13}C (CDCl$_3$) δ 188.5, 187.9, 156.0, 140.7, 136.6, 130.9, 130.6, 127.9, 122.4, 120.8, 113.9, 55.5.

(E)-3-(4-hydroxy-3-nitrophenyl)-1-phenylprop-2-en-1-one **(OHNH)**: **OHNH** was synthesized following the method described in Section 4.2 with acetophenone (120 mg) and 4-hydroxy-3-nitrbenzaldehyde (169 mg). TLC using chloroform: methanol (9:1) as developing solvent. The compound was purified by silica gel column (60-120 mesh) chromatography using chloroform as eluent. Shiny yellow solid. Yield: 203 mg (75%) ^{1}H NMR (400 MHz, CDCl$_3$) δ 9.96 (s, 1H), 8.39 (s, 1H), 8.17-8.14 (dd, J = 2 Hz and J = 2 Hz 1H), 7.78 (d, J = 16 Hz, 1H), 7.61 (d, J = 8 Hz, 2H), 7.56-7.51 (m, 1H), 7.33 (d, J = 8 Hz, 1H), 7.28(d, J = 16 Hz, 1H).

(E)-1-(4-chlorophenyl)-3-(4-methoxyphenyl)prop-2-en-1-one **(COMeCl)**: **COMeCl** was synthesized following the method described in Section 4.2 with 4-chloroacetophenone (155 mg) and anisaldehyde (136 mg). Beige colored solid. Yield: 231 mg (85%). ^{1}H NMR (400 MHz, CDCl$_3$) δ 7.94 (d, J = 8 Hz, 2H), 7.76 (d, J = 16 Hz, 1H), 7.58 (d, J = 8 Hz, 2H), 7.44 (d, J = 8 Hz, 2H), 7.34 (d, J = 16 Hz, 1H), 6.92 (d, J = 8 Hz, 2H), 3.83 (s, 3H).

(E)-1-(4-bromophenyl)-3-(4-(dimethylamino)phenyl)prop-2-en-1-one **(CNBr):** **CNBr** was synthesized following the method described in Section 4.2 with 4-bromoacetophenone (199 mg) and N,N dimethyl-4-aminobenzaldehyde (149 mg). Yellow solid. Yield: 198 mg (60%). ^{1}H NMR (400 MHz, CDCl$_3$) δ 7.86 (d, $J = 8$ Hz, 2H), 7.77 (d, $J = 16$ Hz, 1H), 7.68 (d, $J = 8$ Hz, 2H), 7.61 (d, $J = 8$ Hz, 2H), 7.53 (d, $J = 8$ Hz, 2H), 7.25 (d, $J = 16$ Hz, 1H), 3.01 (s, 6H).

(E)-3-(4-chlorophenyl)-1-(4-methoxyphenyl)prop-2-en-1-one **(PS 10): PS 10** was synthesized following the method described in Section 4.2 with 4-methoxyacetophenone (150 mg) and 4-chlorobenzaldehyde (141 mg). Yellow solid. Yield: 228 mg (84%). ^{1}H NMR (400 MHz, CDCl$_3$) δ 8.02 (d, $J = 8$ Hz, 2H), 7.72 (d, $J = 16$ Hz, 1H), 7.55 (d, $J = 8$ Hz, 2H), 7.50 (d, $J = 16$ Hz, 1H), 7.37 (d, $J = 8$ Hz, 2H), 6.97 (d, $J = 8$ Hz, 2H), 3.89 (s, 3H).

(E)-3-(4-methoxyphenyl)-1-phenylprop-2-en-1-one) **(PS 27)**: **PS 27** was synthesized following the method described in Section 4.2 with acetophenone (120 mg) and 4- methoxybenzaldehyde (136 mg). Yellow solid. Yield: 214 mg (90%). ^{1}H NMR (400 MHz, CDCl$_3$) δ 8.01 (d, $J = 8$ Hz, 2H), 7.78 (d, $J = 16$ Hz, 1H), 7.61 (d, $J = 8$ Hz, 2H), 7.59 (d, $J = 8$ Hz, 2H), 7.51 (t, 3H) 7.41 (d, $J = 16$ Hz, 1H), 3.87 (s, 3H).

(E)-3-(4-dimethyaminophenyl)-1-(4-methoxyphenyl)prop-2-en-1-one **(PS 1)**: **PS 1** was synthesized following the method described in Section 4.2 with 4-methoxyacetophenone (150 mg) and N,N dimethyl-4-amino benzaldehyde (149 mg). Bright yellow solid. Yield: 244 mg (87%). ^{1}H NMR (400 MHz, CDCl$_3$) δ 8.01 (d, $J = 8$ Hz, 1H), 7.76 (d, $J = 16$ Hz, 1H), 7.72 (d, $J = 8$ Hz, 2H), 7.53 (d, $J = 8$ Hz, 2H), 7.33 (d, $J = 16$ Hz, 1H), 6.96 (d, $J = 8$ Hz, 2H), 6.68 (d, $J = 8$ Hz, 1H), 3.88 (s, 6H), 3.04 (s, 3H).

(E)-3-(2-chlorophenyl)-1-(4-methoxyphenyl)prop-2-en-1-one **(PS 16)**: **PS 16** was synthesized following the method described in Section 4.2 with 4-methoxyacetophenone (150 mg) and o-chlorobenzaldehyde (150 mg). Light yellow solid. Yield: 223 mg (82%). ^{1}H NMR (400 MHz, CDCl$_3$) δ 8.13 (d, $J = 16$

Hz, 1H), 8.02 (d, J = 8 Hz, 2H), 7.73 (d, J = 8 Hz, 1H), 7.46 (d, J = 16 Hz, 1H), 7.42 (d, J = 8 Hz, 2H), 7.30 (d, J = 8 Hz, 2H), 6.97 (d, J = 8 Hz, 1H), 3.88 (s, 3H).

(E)-3-(2-chlorophenyl)-1-phenylprop-2-en-1-one **(PS 9)**: **PS 9** was synthesized following the method described in Section 4.2 with acetophenone (120 mg) and o-chlorobenzaldehyde (141 mg). Pale yellow solid. Yield: 205 mg (85%). ^{1}H NMR (400 MHz, CDCl₃) δ 8.10 (d, J = 16 Hz, 1H), 7.94 (d, J = 8 Hz, 2H), 7.67 (d, J = 8 Hz, 2H), 7.51 (d, J = 8 Hz, 1H), 7.40- 7.44 (m, 4H), 7.36 (d, J = 16 Hz, 1H).

(E)-1-(4-(dimethylamino)phenyl)-3-phenylprop-2-en-1-one **(PS 2)**: **PS 2** was synthesized following the method described in Section 4.2 with acetophenone (120 mg) and N,N dimethyl-4-aminobenzaldehyde (149 mg) Orange solid. Yield: 200 mg (80%). ^{1}H NMR (400 MHz, CDCl₃) δ 7.98 (d, J = 8 Hz, 2H), 7.76 (d, J = 16 Hz, 1H), 7.50 (m, 3H), 7.45 (d, J = 8 Hz, 2H), 7.31 (d, J = 16 Hz, 1H), 6.67 (d, J = 8 Hz, 2H), 3.03 (s, 6H).

(E)-1,3-bis(4-methoxyphenyl)prop-2-en-1-one **(PS 5)**: **PS 5** was synthesized following the method described in Section 4.2 with 4- methoxyacetophenone (150 mg) and 4- methoxybenzaldehyde (136 mg). White crystal. Yield: 214 mg (80%). ^{1}H NMR (800 MHz, CDCl₃) δ 8.04 (d, J = 8 Hz, 2H), 7.79 (d, J = 16 Hz, 1H), 7.61 (d, J = 8 Hz, 2H), 7.44 (d, J = 16 Hz, 1H), 6.99 (d, J = 8 Hz, 2H), 6.94 (d, J = 8 Hz, 2H), 3.90 (s, 3H), 3.87 (s, 3H).

(E)-3-(4-chlorophenyl)-1-phenylprop-2-en-1-one **(PS 4)**: **PS 4** was synthesized following the method described in Section 4.2 with 4-chlorobenzaldehyde (141 mg) and acetophenone (120 mg). Pale yellow solid. Yield: 77 %. ^{1}H NMR (800 MHz, CDCl₃) δ 8.20 (d, J = 16 Hz, 1H), 8.03 (d, J = 8 Hz, 2H), 7.76 (d, J = 8 Hz, 2H), 7.61 (t, J = 8 Hz, 1H), 7.50 (d, J = 16 Hz, 1H), 7.52 (d, J = 8 Hz, 1H), 7.45-7.46 (broad m, 1H), 7.33 (t, J = 8 Hz, 2H).

4.4 Synthesis of hydrazone derivatives from chalcone:

General synthetic method: Chalcone derivative (1mmol) was dissolved in ethanol and (2,4-dinitrophenyl)hydrazine (1mmol) was added to it. A catalytic amount of acetic acid was poured into the reaction mixture and refluxed for appropriate time (provided in Table 4.2); precipitate obtained was washed with ethanol.
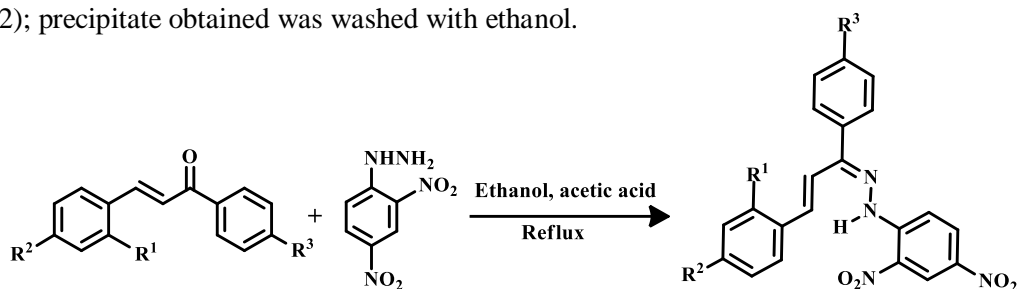
Scheme 4.2: Synthesis of hydrazone derivatives of chalcone.

Table 4.2: Physical data of hydrazone derivatives of chalcone.

Compound & Code	Time	M.P. (℃)	Compound & Code	Time	M.P. (℃)
PS 6	20 min	245-246	PS 21	25 min	169-170
PS 7	35 min	240-241	PS 8	4 h	200-203
PS 18	25 min	213-214	PS 22	30 min	230-232

4.5 Characterization of hydrazone derivatives:

Fig. 4.3 shows the ^{1}H-NMR (400 MHz, CDCl$_3$) spectrum of *(E)-1-((E)-3-(2-chlorophenyl)-1-phenylallylidene)-2-(2,4-dinitrophenyl)hydrazine* **(PS 7)**, The structure of the compound is in Fig. 4.3a. and Fig. 4.3b shows the region 7.0 -9.1 ppm.
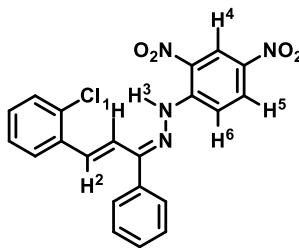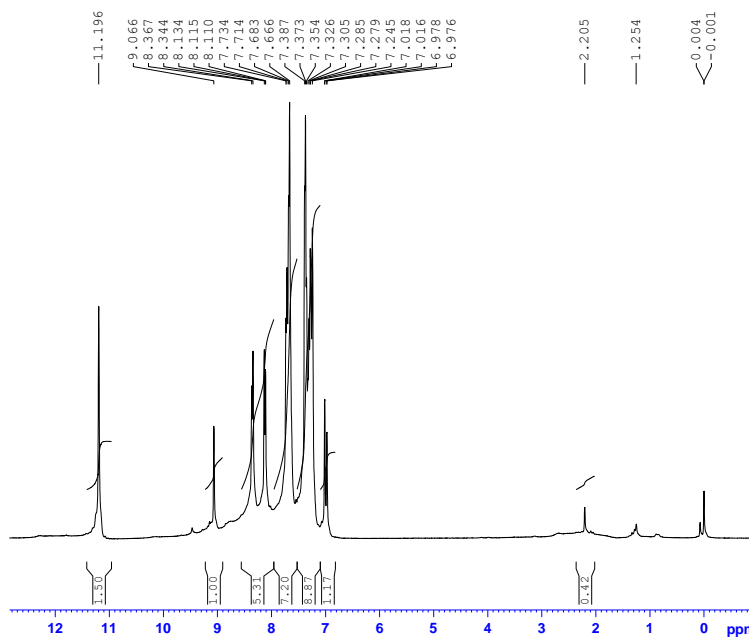

Figure 4.3a: PS 7

Figure 4.3: ^{1}H NMR spectrum of *(E)-1-((E)-3-(2-chlorophenyl)-1-phenylallylidene)-2-(2,4-dinitrophenyl)hydrazine* (**PS 7**).
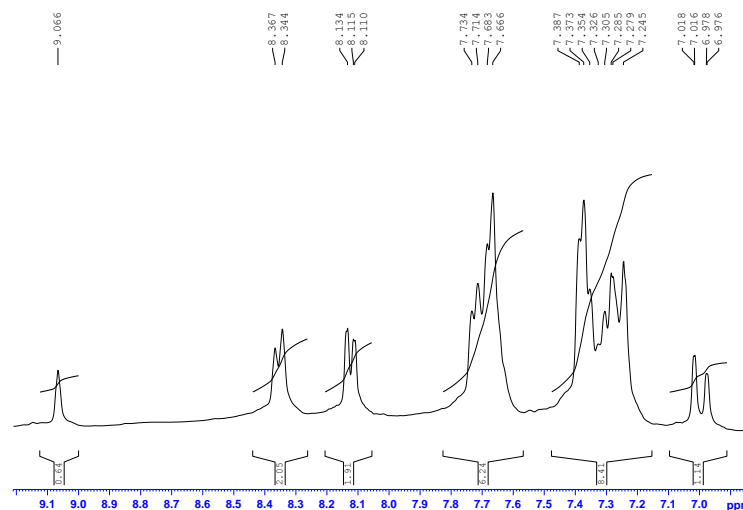
Figure 4.3b: ^{1}H NMR spectrum of *(E)-1-((E)-3-(2-chlorophenyl)-1-phenylallylidene)-2-(2,4-dinitrophenyl)hydrazine* (**PS 7**), region 7.0-9.1 ppm.

Here the olefin H^1 & H^2 protons of the compound appeared as two distinct doublets centered at $\delta = 7.26$ ppm and $\delta = 6.98$ ppm respectively with coupling constant $J = 16$ Hz. The aromatic protons in the phenyl ring resonated as distinct doublets centered at $\delta = 8.12$ ppm $J = $ Hz and $\delta = 7.73$-7.66 ppm as multiplet for four protons. One of the aromatic protons H^4 present in the dinitrophenyl ring appeared as a singlet at $\delta = 9.06$ ppm. The H^5 & H^6 proton of the same ring resonated as a doublet centered at $\delta = 8.35$ ppm with the coupling constant $J = 9.6$ Hz. The NH proton, H^3, appeared as a singlet at $\delta = 11.19$ ppm. The characteristic NMR signals observed in the spectrum confirm the structure of the compound.

PS 7 has been taken as a representative compound of the series. The spectra of other compounds in the series are available in the Section 4.16.

(E)-1-((E)-3-(4-chlorophenyl)-1-phenylallylidene)-2-(2,4-dinitrophenyl)hydrazine (**PS 6**): **PS 6** was synthesized from **PS 4** [*(E(3-(4-chlorophenyl)-1-phenylprop-2-en-1-one)*] (242 mg) and (2,4-dinitrophenyl)hydrazine (198 mg) following the procedure discussed in Section 4.4.Orange solid. Yield: 295 mg (70%). ^{1}H NMR (400 MHz, CDCl$_3$): δ 11.10 (s, 1H), 9.02 (s, 1H), 8.34 (d, $J = 9.6$ Hz, 1H), 8.13 (d, $J = 8$ Hz, 2H), 7.67-7.63 (m, 4H),7.28-7.52 (m, 4H) 7.26 (d, $J = 16$ Hz, 1H), 6.49 (d, $J = 16$ Hz, 1H).

(E)-1-((E)-3-(2-chlorophenyl)-1-phenylallylidene)-2-(2,4-dinitrophenyl)hydrazine **(PS 7)**: **PS 7** was synthesized from **PS 9** *[(E)-(3-(2-chlorophenyl)-1-phenylprop-2-en-1one)]* (242 mg) and (2,4-dinitrophenyl)hydrazine (198 mg) following the procedure discussed in Section 4.4. Red solid. Yield: 303 mg (72%). ^{1}H NMR (400 MHz, CDCl$_3$): δ 11.19 (s, 1H), 9.06 (s, 1H), 8.35 (d, J = 9.6, 1H), 8.12 (d, J = 8, 2H), 7.73-7.66 (m, 4H), 7.38-7.30 (m, 4H), 7.26 (d, J = 16 Hz, 1H), 6.98 (d, J = 16, 1H).

4-((1E,3E)-3-(2-(2,4-dinitrophenyl)hydrazono)-3-phenylprop-1-en-1-yl)-N,N-dimethylaniline **(PS 18)**: **PS 18** was synthesized from **PS 2** [*(E)-3-(4-(dimethylaminophenyl)-1-phenyl prop-2-en-1-one*] (251 mg) and (2,4-dinitrophenyl)hydrazine (198 mg) following the procedure discussed in Section 4.4. Black solid. Yield: 323 mg (75%). ^{1}H NMR (400 MHz, CDCl$_3$): δ 11.09 (s, 1H), 9.03 (s, 1H), 8.29 (d, J = 9.6 Hz, 1H), 8.02 (d, J = 8 Hz, 2H), 7.63 (m, 2H), 7.26-7.34 (m, 3H), 7.07 (d, J = 16 Hz, 1H), 6.70-6.64 (m, 3H), 6.45 (d, J = 16 Hz, 1H), 3.01 (s, 6H).

(E)-1-((E)-1,3-bis(4-methoxyphenyl)allylidene)-2-(2,4-dinitrophenyl)hydrazine **(PS 21)**: **PS 21** was synthesized from **PS 5** [*(E)-1,3-bis(4-methoxyphenyl)prop-2-en-1-one*] (268 mg) and (2,4-dinitrophenyl)hydrazine (198 mg) following the procedure discussed in Section 4.4. Red solid. Yield: 295 mg (66 %). ^{1}H NMR (400 MHz, CDCl$_3$): δ 11.21 (s, 1H), 9.06 (s, 1H), 8.32 (d, J = 8 Hz, 1H), 8.09 (d, J = 8 Hz, 1H), 7.72 (d, J = 8 Hz, 1H), 7.53 (d, J = 8 Hz, 1H), 7.39 (d, J = 8 Hz, 2H), 7.13 (d, J = 16 Hz, 1H), 7.03-6.95 (m, 2H), 6.88 (d, J = 8 Hz, 2H), 6.52 (d, J = 16 Hz, 1H), 3.92 (s, 3H), 3.83 (s, 3H).

4-((1E,3E)-3-(2-(2,4-dinitrophenyl)hydrazono)-3-(4-methoxyphenyl)prop-1-en-1-yl)-N,N dimethylaniline **(PS 22)**: **PS 22** was synthesized from **PS 1** [*(E)-3-(4-dimethyaminophenyl)-1-(4-methoxyphenyl)prop-2-en-1-one*] (281 mg) and (2,4-dinitrophenyl)hydrazine (198 mg) following the procedure discussed in Section 4.4. Black solid. Yield: 350 mg (76%). The compound is present in both *cis* and *trans* configuration. ^{1}H NMR (400 MHz, CDCl$_3$): δ 11.35 (s, 1H), 9.05 (s, 1H), 8.32 (d, J = 8 Hz, 1H), 8.09 (m, 2H), 7.83 (d, J = 8 Hz, 1H), 7.70 (d, J = 8 Hz,

1H), 7.63 (d, *J* = 8 Hz, 1H), 7.30 (d, *J* = 16 Hz, 1H), 6.99-6.91 (m, 2H)**,** 6.73-6.44 (m, 2H), 6.50 (d, *J* = 16 Hz, 1H), 3.04 (s, 3H), 3.89 (s, 3H).

(E)-1-((E)-3-(4-chlorophenyl)-1-(4-methoxyphenyl)allylidene)-2-(2,4 dinitrophenyl)hydrazine **(PS 8**): **PS 8** was synthesized from **PS 10** [*(E)-3-(4-chlorophenyl)-1-(4-methoxyphenyl)prop-2-en-1-one*] (272 mg) and (2,4-dinitrophenyl)hydrazine (198 mg) following the procedure discussed in Section 4.4. Red solid. Yield: 352 mg (78%). The compound is present in both *cis* and *trans* configuration. ^{1}H NMR (400 MHz, CDCl$_3$): δ 11.24 (s, 1H), 9.07 (s, 1H), 8.36 (d, *J* = 9.6 Hz, 1H), **7.75** (d, *J* = 8 Hz, 2H), 7.42 (d, *J* = 8 Hz, 2H), 6.99 (d, *J* = 8 Hz, 2H),7.52 (d, *J* = 8 Hz, 2H), 7.75 (d, *J* = 8 Hz, 2H), 7.34 (d, *J* = 16 Hz, 1H), 7.05 (d, *J* = 16 Hz, 1H), 3.89 (s, 3H).

4.6 Linear optical properties of chalcone derivatives:

The absorption and emission spectra of all the compounds were recorded in chloroform at room temperature with 0.5×10^{-8} M concentration. The photophysical data of chalcones (synthesized with Scheme 4.1) is provided in Table 4.3, absorption and emission spectra of some compounds are presented in Fig. 4.4 and Fig. 4.5 respectively. The excitation wavelength is given in bracket (see Table 4.3).

Table 4.3: Photophysical data of chalcone derivatives.

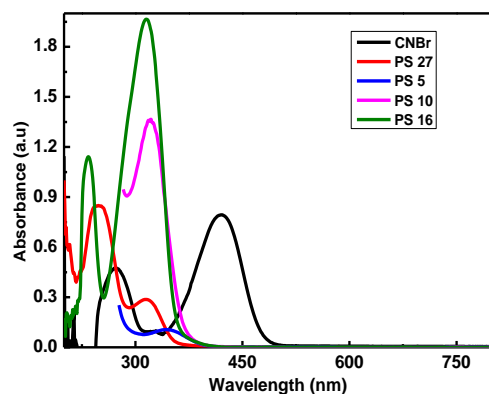| Compound	λ_{abs} (nm)	λ_{em} (nm)	Compound	λ_{abs} (nm)	λ_{em} (nm)
PS10	320, 284	377(322)	**PS 1**	409	505 (408)
PS16	315, 234	377 (320)	**PS 4**	293	355 (296)
PS5	347	409 (337)	**PS 9**	293	350 (295)
PS 27	317, 249	410 (338)	**PS 2**	414	515 (412)
CNBr	420, 273	397, 442 (270)	**COMeCl**	344	431 (343)

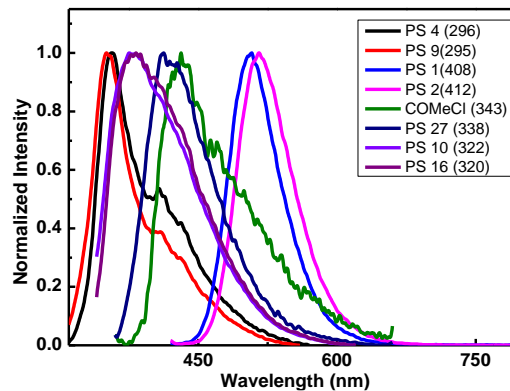**Figure 4.4: Absorption spectra of chalcone derivatives.**

Figure 4.5: Emission spectra of chalcone derivatives.

Two characteristic spectral band due to $n - \pi^*$ and $\pi - \pi^*$ was obtained for most of the compounds. **CNBr** has the highest absorption maxima (λ_{abs}) at 420 nm; as — N(CH$_3$)$_2$ donor group is present in its ring B, which increases the conjugation length & red shifted the absorption maxima.

4.7 Solvatochromism study:

Four chalcone derivatives (**OHNH**, **OHNBr**, **OHNCl,** and **OHNMe**) were specially designed and selected for solvatochromic studies. The absorption spectra for these chalcones were recorded in hexane, chloroform & acetone at room temperature. Fig. 4.6 contains the absorption spectra in chloroform. The effect of solvent on their absorption maxima is gathered in Table 4.4. All other photophysical spectra are available in the Section 4.16.

Table 4.4: Photophysical data of OHNH, OHNMe, OHNCl, and OHNBr.

Compound	Absorbance maxima (nm)			
	SOLVENT SYSTEM			
	Hexane	Chloroform	Acetone	Ethanol
OHNH	306, 360	257, 376	329, 384	255, 325
OHNMe	313, 376	321, 393	330, 393	272, 325
OHNCl	310, 375	316, 386	328	270, 324
OHNBr	310, 378	317, 389	330, 386	274, 322
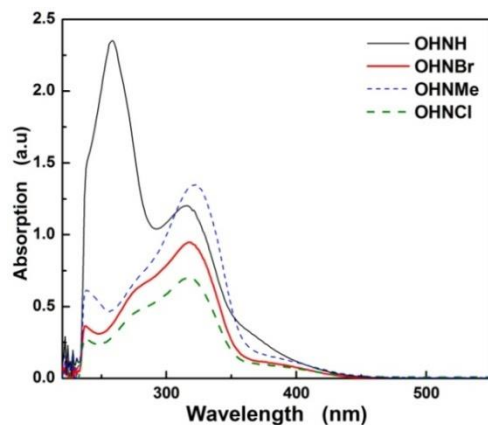
Figure 4.6: Absorption spectra of **OHNH, OHNMe, OHNCl,** and **OHNBr** in chloroform.

The UV spectra show a bathochromic shift in the absorbance maxima with an increase in solvent polarity (hexane→ chloroform→ acetone) and the presence of two characteristic spectral bands ($n - \pi^*$, $\pi - \pi^*$ transition) of carbonyl compounds. When the solvent polarity was further increased to ethanol the absorption maximum did not show any red shift.

4.8 Excitation Dependent Fluorescence (EDF) studies of the compounds:

To study the excitation-dependent fluorescence (EDF), emission spectra were recorded by varying the excitation wavelength from 310 nm to 450 nm with a 10 nm interval. With a gradual increase in the excitation wavelength, the emission wavelength of all the compounds also increased, this effect is known as Red-edge effect. As emission was dependent on excitation wavelength, this is a violation of Kasha's rule. A representative compound, **OHNBr** in Fig. 4.7 shows the EDF in hexane; plot for other compounds are in the Section 4.16. This unique property can be explained by the knowledge that fluorescence is a haphazard event, where fluorophore emits at different times & the decay rate is nothing but the average of a group of fluorophores. The energy levels of these compounds are probably close enough, which increases the possibility of transition of an electron in the higher energy levels. This densely spaced electronic state makes it easier for the transiting electrons to "*always*" get an appropriate energy level available even with a shift in excitation frequency. Consequently, fluorescence behavior and variable light emitting property are also imparted in this series of compounds.
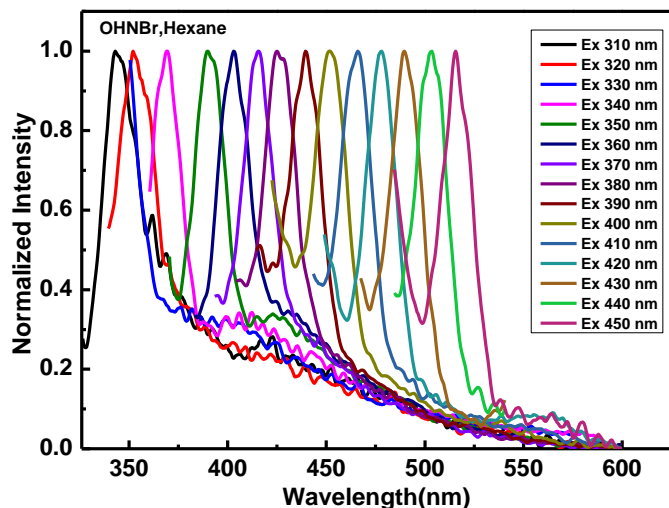
**Figure 4.7:** Exhibition of excitation dependent fluorescence with continuous red shift of OHNBr in hexane.

The continuous spectral shift showed no change in spectral shape. These fluorophores are typically more tightly hydrogen-bonded to the solvent; the shift occurs due to emission from the unrelaxed state. In the process of solvent relaxation, some molecules are partially relaxed but are able to emit energy and returns to the G.S. Gradually, more of the molecules got relaxed and displayed a red-shifted emission.

4.9 Exhibition of dual emission peak of chalcones through Twisted Intramolecular Charge Transfer (TICT):

Molecules in which one part acts as an electron acceptor and another as electron donor generally exhibit TICT states. Upon photoexcitation, intramolecular charge transfer occurs between the donor and the acceptor part of the molecule.
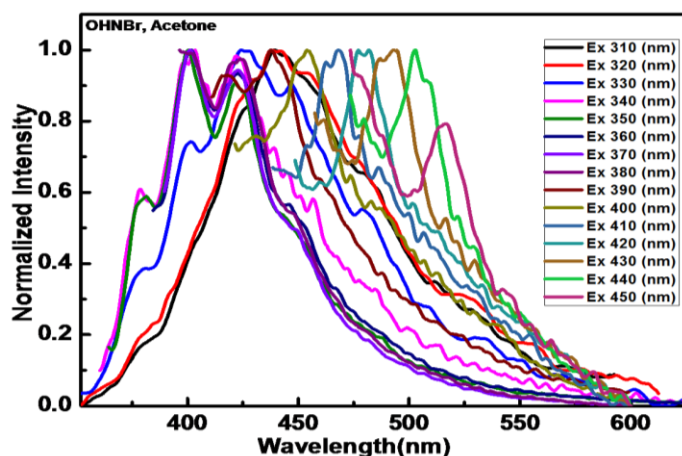
Figure 4.8: TICT spectra of OHNBr in acetone.

Importantly, this charge-transfer is dependent on the ability of the molecule to twist, mostly from an all-planar geometry to 90 degree twisted geometry [3].

The emission spectra of **OHNBr** exhibited the dual peak in acetone, due

to twisted intramolecular charge transfer complex formation, especially when excited with 340-360 nm (Fig. 4.8).

The photophysical properties of such TICT complexes depend on their environment. In the present molecular system, the electron donor and electron withdrawing moieties are coupled through a motif of alternating single and double bonds. The two units can rotate relative to each other. The extent of charge transfer was tuned through the incorporation of -OH, $-NO_2$, and –Br, –H. After photon absorption, in the excited-state, this rotation or twisting motion alters the fluorescence emission characteristics. De-excitation from the TICT state occurs at a lower energy level and lead to a red-shifted second emission peak. As polar solvents promote the shift of the molecule from its local excited (LE) state into a TICT state by twisting around a single bond, two-peak emission in the present cases has been observed with acetone as the solvent [4,5]

4.10 Nonlinear optical properties of chalcone derivatives:

Fig. 4.9 shows the open aperture data of z-scan measurements with 532 nm beam for **OHNH**, **OHNCl**, **OHNBr** and **OHNMe**. The laser pulse energy was $\approx$ 570 μJ. The transmission well away from the focal point of the beam (larger z values) is nearly one because the samples do not have much absorption at low intensities near 532 nm. But, near the focal point the transmission of the samples reduces and reaches a minimum at $z = 0$. Nonlinear absorption is responsible for this lowering of transmission at higher intensities.
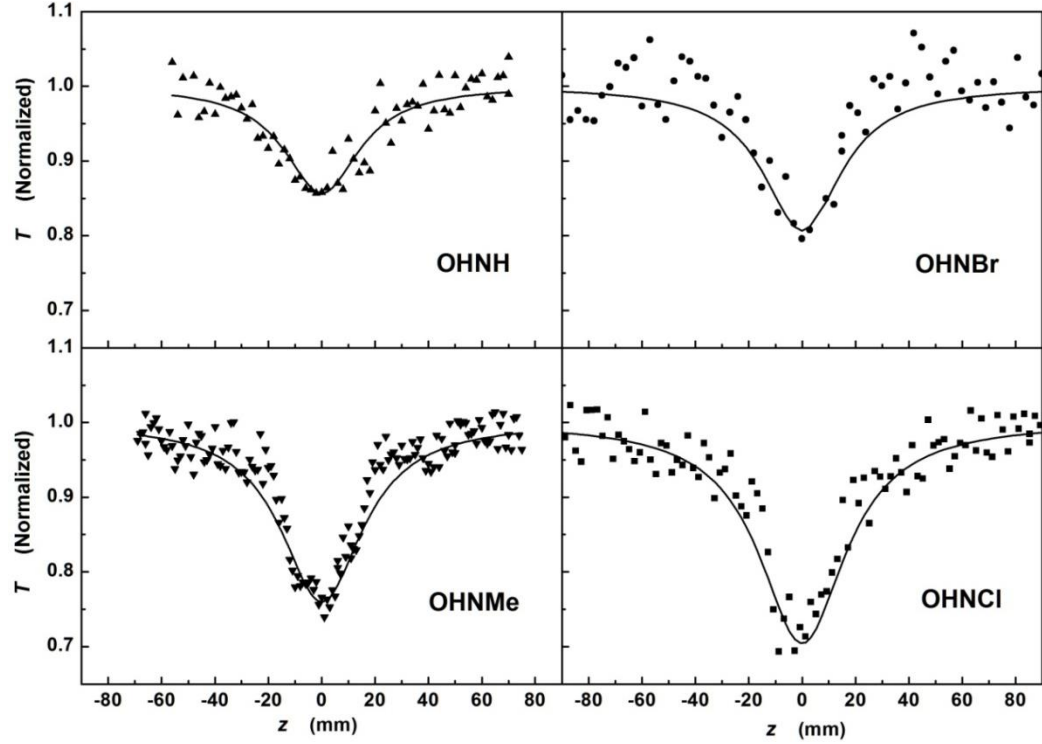
Figure 4.9: Open aperture z-scan data of all the four chalcone materials measured with per pulse energy ~570 µJ. Solid lines are the best fit to the data using Eqn.4.3.

The rate of change in intensity (I) as the beam propagates through the sample, not having linear absorption, can be written as

$$\frac{dI}{dz} = -\beta I^2 \tag{4.1}$$

Where β is the nonlinear absorption coefficient related to the third-order susceptibility of the sample. For a Gaussian intensity distribution (in space and time), the sample is at z, the intensity distribution, I, at the entrance side of the sample is given by,

$$I(r,t,z) = \frac{I_0}{1+(z/z_0)^2} \exp[-2(r/\omega_0)^2 - (t/t_0)^2] \tag{4.2}$$

Where ω_0 is the beam radius, t_0 refers to pulse width and z_0 (Rayleigh range) = $\pi\omega_0^2/\lambda$ and λ is the wavelength of light used. Using Eqn. 4.1 and 4.2 the energy of the pulse transmitted through the sample can be obtained by integration over space and time and is given by [6],

$$T(z) = \frac{1}{\sqrt{\pi}q(0,0,z)} \int_{-\infty}^{\infty} \ln\left[1 + q(0,0,z)\exp\left(-\tau^2\right)\right] d\tau$$

(4.3)

where, $q(r,t,z) = \beta I(r,t,z)L$, L denotes the thickness of the sample. The experimental z-scan data was fit to Eqn. 4.3 by solving it numerically with β as the fitting parameter. The obtained best-fit values of β are tabulated in Table 4.5 together with the band gap of the materials. **OHNCl** showed the maximum β nearly 3 times more than that of the lowest; **OHNH**. Since the samples show emission at 532 nm, there is some states present which can absorb the wavelength at which the z-scan experiment was performed. At high intensities, these carriers which are excited by absorption of a single photon of the 532 nm light may further get excited to the deeper state near to 266 nm. So, the measured nonlinear absorption is two-step two-photon absorption.

However, the nonlinear absorption of all the compounds was nearly of the same order, so correlation of the NLA with electron donating or withdrawing effects cannot be drawn. On an average, the nonlinear absorption coefficient is much higher as compared to some of the samples of similar genre.

4.11 Band Gap Calculation: For the estimation of optical energy gap, the photon energy dependence of $(\alpha h\upsilon)^{1/2}$ (the Tauc's plot of indirect materials), was estimated from the absorption spectrum of the samples, α is the linear absorption coefficient, h is the Planck's constant and υ is the optical frequency. The dual slope behavior of the Tauc plot near the band edge clearly shows that the present materials has indirect bandgap [7, 8] (Fig. 4.10). and in these materials both the band gap (E_g) and phonon characteristic energy (E_p) defines the variation of linear absorption with incident photon energy. So, E_g and E_p were estimated and the values are arranged in Table 4.5 and Fig. 4.10 shows the Tauc's plot.

Table 4.5: Nonlinear absorption coefficient, band gap (E_g) and phonons characteristic energies (E_p) of the compounds.

Compound	E_g (eV)	E_p (eV)	β (cm/GW)
OHNH	2.9	0.25	11.5
OHNBr	2.96	0.34	17
OHNMe	2.89	0.37	22
OHNCl	2.88	0.41	32
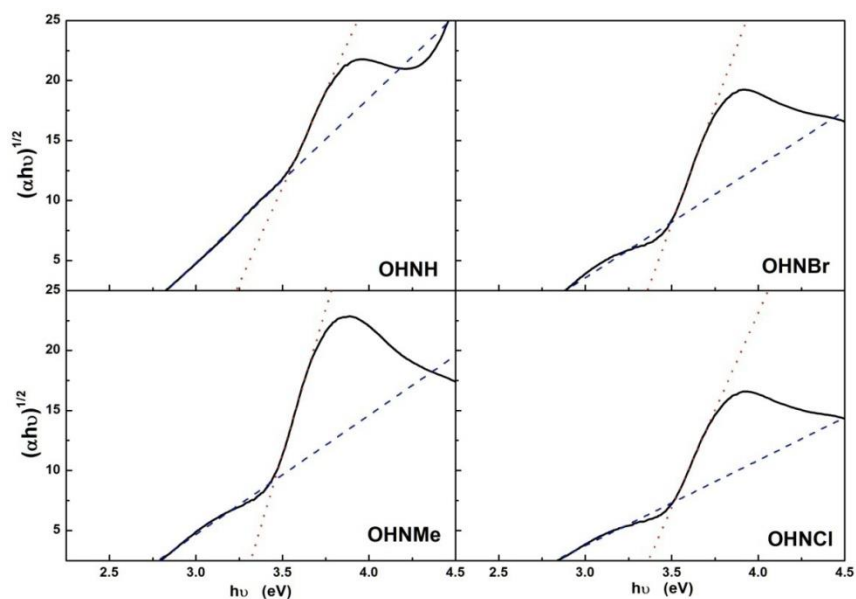
Figure 4.10: Tauc plot of the **OHNH**, **OHNMe**, **OHNBr** and **OHNCl** for the estimation of the band gap. The solid line is the experimental data. Blue dashed lines and red dotted lines are the linear fit to the part of the data to estimate the values of (E_g - E_p) and (E_g+E_p) from which the values of E_g and E_p are estimated.

The nonlinear absorption of the four *(E)-1-(4-substitutedphenyl)-3-(4-hydroxy-3-nitrophenyl)prop-2-en-1-one* compounds do not show any consistent variation with the bandgap of the material (See Table.4.5). However, the nonlinear absorption clearly increases exponentially with the increase in photon

characteristic energies (E_p). Fig. 4.11(a) shows the variation of nonlinear absorption of the four compounds with the phonon characteristic energies. From
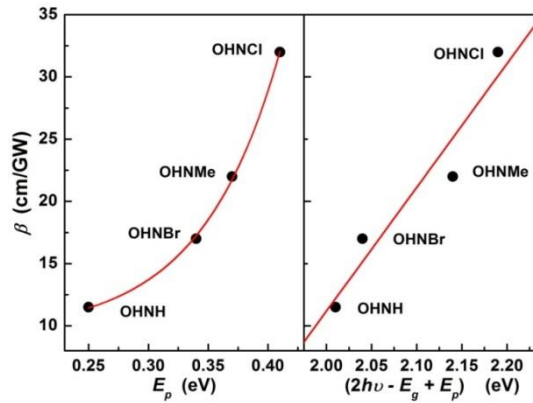
Figure 4.11: Variation of nonlinear absorption of **OHNH, OHNBr, OHNCl** and **OHNMe** with the **(a)** phonon characteristic energies, *Ep*, and **(b)** $(2h\upsilon - Eg + Ep)$. The red lines are the best fit to the data with an exponential growth function and linear.

Fig. 4.11(b) it is clear that the nonlinear absorption increases exponentially with the increase in photon characteristic energies. It has been shown earlier that phonons can play a strong role in the nonlinear absorption in different kinds of materials [9-13]. Hence the phonons play a strong role in the nonlinear absorption observed in the present chalcones in the nanoseconds time scale. The dependence of two-photon absorption on the indirect band gap of bulk semiconductors and semiconductors confined in one and two dimensions was theoretically studied by A. R. Hassan [14] and it was showed that the two-photon absorption coefficient scales as a function of $(2h\upsilon - E_g + E_p)^{\sigma}$ where υ is the operating frequency, σ depends on the dimensions of the semiconductor. Chalcones are very different from semiconductors, still, to find out the relation between NLA and $(2h\upsilon - E_g + E_p)$ was investigated. It was observed that the nonlinear absorption coefficients of the compounds increases with increase in $(2h\upsilon - E_g + E_p)$.

The nonlinear absorption coefficient (β) of other chalcones are presented in Table 4.06 and the open aperture z-scan data are available in Section 4.16.

Table 4.06: Open aperture z-scan data of chalcone derivatives.

Compound	β (cm/GW)	Compound	β (cm/GW)
PS 1	3.357	PS 16	1.59
PS 9	2.29	PS 10	2.11
PS 5	0.027	PS 2	0.047

4.12 Linear optical properties of hydrazone derivatives of chalcone:

The absorption and emission spectra were recorded in chloroform at room temperature with 0.9×10^{-8} M concentration. Table 4.6 gathers the photophysical data of six hydrazone derivatives.

Table 4.6 Photophysical data of hydrazone derivatives of chalcone.

Compound	λ_{abs} (nm)	λ_{em} (nm)	Compound	λ_{abs} (nm)	λ_{em} (nm)
PS18	436, 336	556 (435)	PS 7	396, 306	537 (396)
PS22	434, 359	515 (436)	PS 6	396, 312	531 (394)
PS21	410, 324	584 (410)	PS8	402, 311	521 (397)
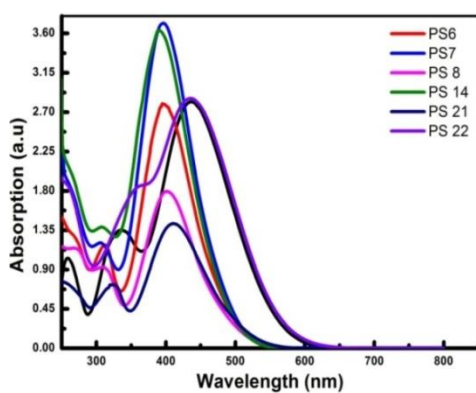
Figure 4.12: Absorption spectra of hydrazone derivative of chalcones**.**
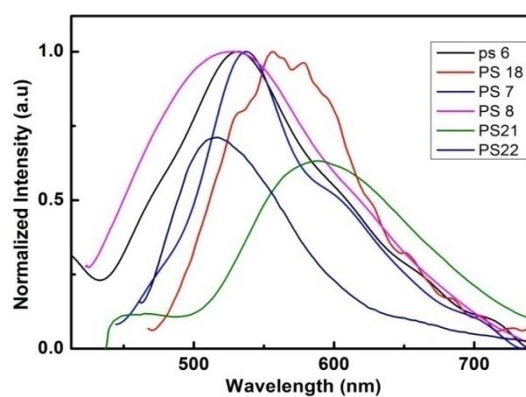
Figure 4.13: Emission spectra of hydrazone derivative of chalcones.

Fig. 4.12 shows the absorption spectra of the hydrazone derivatives. The emission

spectra of the compounds, when excited at their absorption maxima, is shown in Fig. 4.13. The peaks observed are attributed to $n - \pi^*$ interband transition and are due to the excitation in the aromatic rings. Due to the presence of dinitro chromophore on the other ring, absorption peaks ~ 390-400 nm, 306-336 nm are observed [15, 16]. The region between 450-850 nm is transparent and all the compounds are fluorescent in nature. A bathochromic shift is observed for **PS 18** in comparison to other compounds in the series due to the presence of —N(CH$_3$)$_2$ group in ring (directly in conjugation with the ethylenic part) of **PS 18**. But the presence of —OCH$_3$ in the other ring along with —N(CH$_3$)$_2$ group in **PS 22** did not red shifted the absorption maxima as compared to **PS 18.**

4.13 Nonlinear optical properties:

Two-photon absorption coefficient of hydrazones are provided in Table 4.7. The experimental data was fitted to Eqn. 4.3. A comparative study of the synthesized hydrazone derivatives was done to understand the structure-property relationship of their nonlinear absorption.

Table 4.7: Two-photon Absorption Coefficient of hydrazone derivatives.

Code	β(cm/GW)	Code	β(cm/GM)
PS 22	5.05	**PS 8**	0.67
PS 6	6.65	**PS 18**	5.17
PS 7	5.69	**PS 21**	4.02
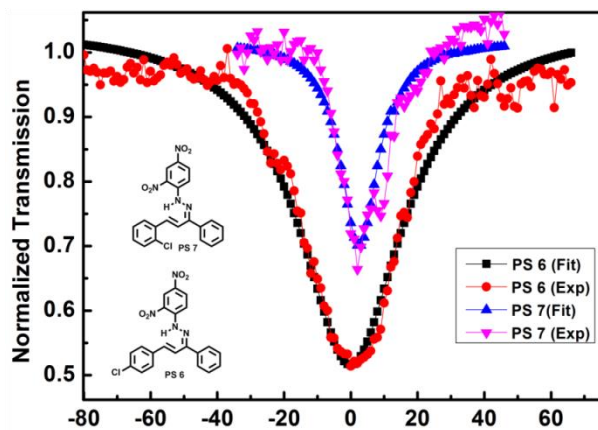
Figure 4.14: Open apperture z scan data PS 6 and PS 7.

The motif for **PS 6** and **PS 7** compounds could be seen as $D - \pi - A - D$ or $A - \pi - A - D$ as -Cl group can act both as a donor and acceptor (i.e., amphiprotic) depending upon the strength of other substituent present in the segment. The only difference

between the two compounds is in the position of –Cl group, in **PS 6** the –Cl group is in the para position of the phenyl ring and **PS 7** has the –Cl group is in the ortho position. As it is known that the electron delocalisation by the –Cl group in the para position is more than that of ortho position. So, -Cl acts as a donating group and the motif is in $D - \pi - A - D$ the arrangement.This structural change brings about large enhancement in the nonlinear absorption. Fig 4.14 shows the open aperture z-scan data of the two compounds.

Figure 4.15 shows open aperture z scan data of **PS 18** and **PS 22. PS 18** and **PS 22** both the compounds have N,N-dimethyl group as a donor. In **PS 18** the motif is $D - \pi - A - \pi - D$ and in **PS 22**, $D - \pi - A - \pi - D$ as **PS 22** has an additional –OCH$_3$ group attached to ring B in it. This –OCH$_3$ group was introduced to increase the electron delocalisation in the system. It was expected that increase in electron density would, in turn, increase the NLA. But the present scenario is quite
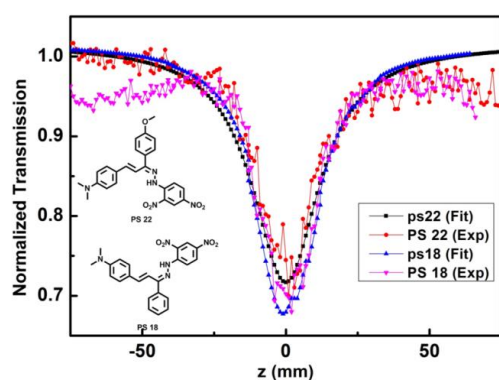
Figure 4.15: Open aperture z scan data PS 18 and PS 22

different from that. Chalcones are cross-conjugated molecules, and the carbonyl group in these systems breaks the conjugation system into two independent parts to have a 2D β character. It could be concluded that the incorporation of –OCH$_3$ was not fruitful in the enhancement of NLA.

Figure 4.16 shows open aperture z scan data of **PS 8** and **PS 21. PS 8** and **PS 21** differs in their structure in two ways- (a) –OCH$_3$ group is replaced with –Cl group but the position of the group is not changed. The explanation of the increased TPA coefficient is again the delocalisation of electrons and charge transfer. Though the p-Cl group is donating is nature but it is less effective than the p-methoxy group. Naturally, with more labile electron delocalisation, the change in polarization would be more and also the NLA.
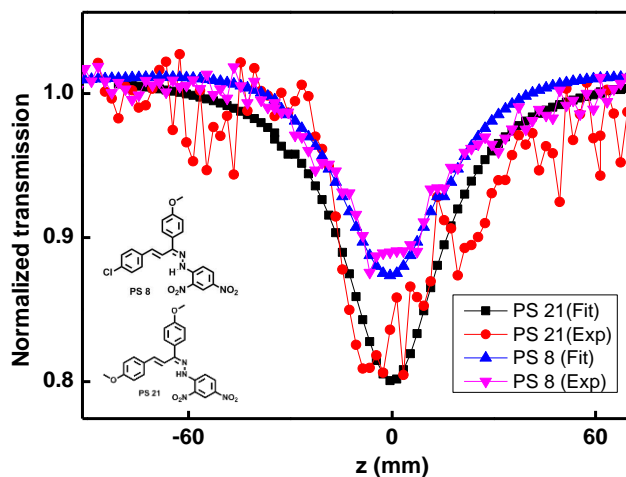
Figure 4.16: Open aperture z scan data PS 8 and PS 21.

4.14 Conclusion:

A total of 14 chalcones and 6 hydrazone derivatives have been synthesized through green chemistry and all of them had nonlinear optical properties. The synthesized series of *(E)-1-(4-substitutedphenyl)-3-(4-hydroxy-3-nitrophenyl)prop-2-en-1-one* exhibited uncommon excitation-dependent emission, this scope of the materials for potential use as multi-wavelength fluorophore in biological imaging is expected. In this series, the indirect band gap was also calculated from the absorption data using Tauc's plot. The hydrazones exhibited NLO property and *(E)-1-((E)-3-(4-chlorophenyl)-1-phenylallylidene)-2-(2,4-dinitrophenyl)hydrazine* had very high two-photon absorption coefficient of 6.65 cm/GW. The detailed absorption and emission characteristic were studied to know the electronic properties.

4.15 References:

1. Sharma, R.N.; Sharma, K.P.; Dixit, S.N. *Der Chemica Sinica*. **2010**. *1 (1)*. 57.
2. Choi, E.Y.; Kim, P.J.; Jazbinsek, M.; Kim, J.T.; Lee, Y.S.; Gunter, P.; Lee, S. W.; Kwon, O.P. *Cryst. Growth Des.* **2011**. *11*. 3049.

3. Ionita, P. *S. Afr. J. Chem*. **2008**. *61*. 123.

4. Al-Hassan, K.A. *J. Fluoresc*. **2013**. *23*.1197.

5. Haidekker, M.A.; Brady, T.P.; Lichlyter, D.; Theodorakis, E.A. *Bioorg. Chem*. **2005**. *33.* 415.

6. Said, A.A.; Sheik-Bahae, M.; Hagan, D.J.; Wei, T.H.; Wang, J.; Young, J.; W Van Stryland, E. *J. Opt. Soc. Am. B*. **1992**. *9.* 405.

7. Pankove, J.I. *Optical processes in semiconductors*, Dover Publications, Inc. New York. **1971**.

8. Tauc, J. *The Optical Properties of Solids*. Academic Press, New York. **1966**. 1966.

9. Baev, A.; Polyutov, S.; Minkov, I.; Gelmukhanov, F.; Gren, H. *Non-Linear Optical Properties of Matter: From Molecules to Condensed Phase*, Springer, The Netherlands. **2006**. *Ch. 6: Non-Linear Pulse Propagation in Many-Photon Active Isotropic Media.* pp. 211-250.

10. Stafford, R.G.; Park, K. *Phys. Rev. B.* **1971**. *4.* 2006.

11. Gal'perin, Y.M.; Gurevich, V.L.; Parshin, D.A. *Sov. Phys. JETP*. **1984**. *60* 1259.

12. Frhlich, D.; Rbenacke, S.; Schlutt, C.; Stolz, H. *Phys. stat. sol. (b).* **1995**. *190.* 241.

13. Garcia, H.; Kalyanaraman, R. *J. Phys. B: At. Mol. Opt. Phys*. **2006**. *39*. 273.

14. Hassan, A.R. *Phys. stat. sol. (b)*. **1994**. *184*. 519.

15. Sawant, B.A.; Nirwan, R.S. *Indian J Pure. Appl Phys*. **2012**. *50.* 308.

4.16 Spectral data:
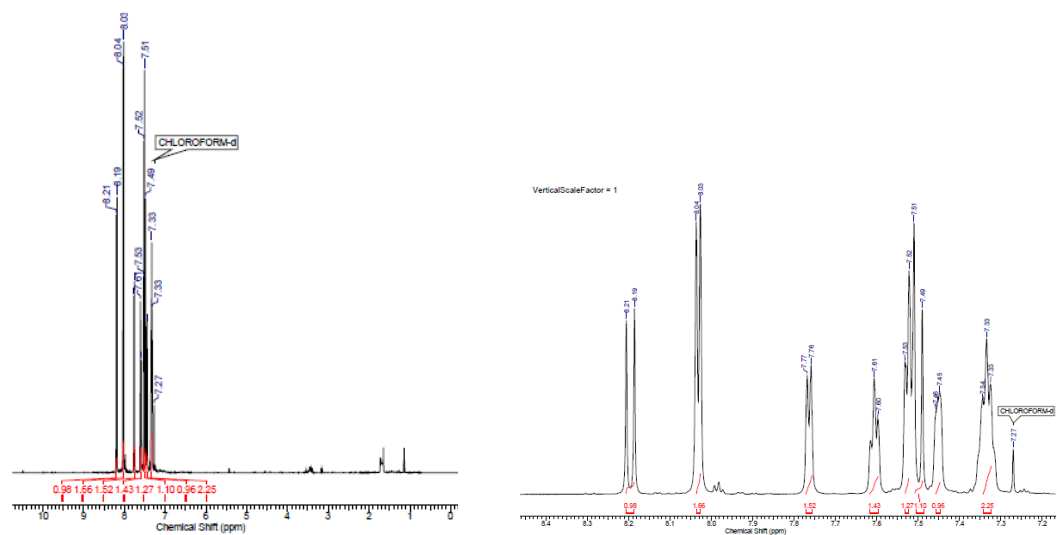
Figure 4.17: ¹H NMR spectrum of *(E)-3-(4-chlorophenyl)-1-phenylprop-2-en-1-one* (PS 4).
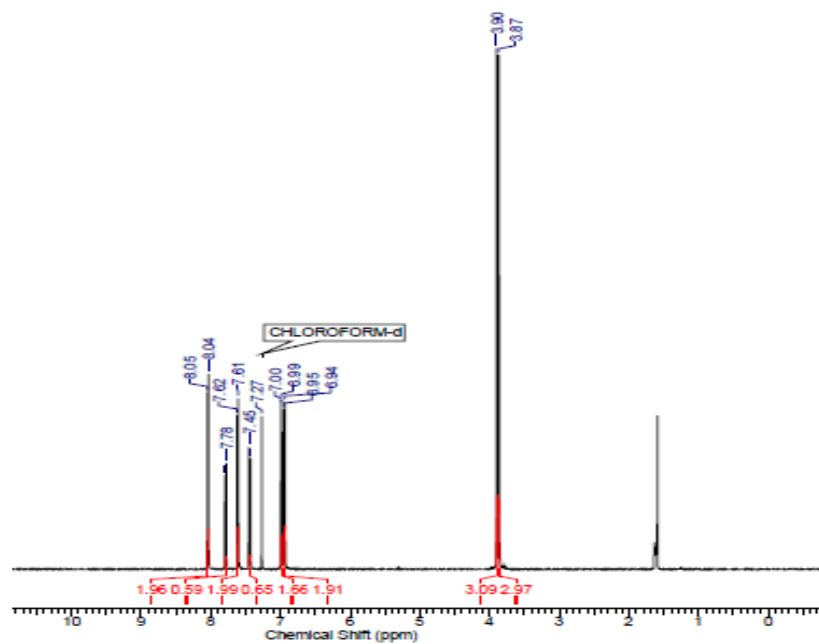
Figure 4.18: ¹H NMR spectrum of *(E)-1,3-bis(4-methoxyphenyl)prop-2-en-1-one* (PS 5).
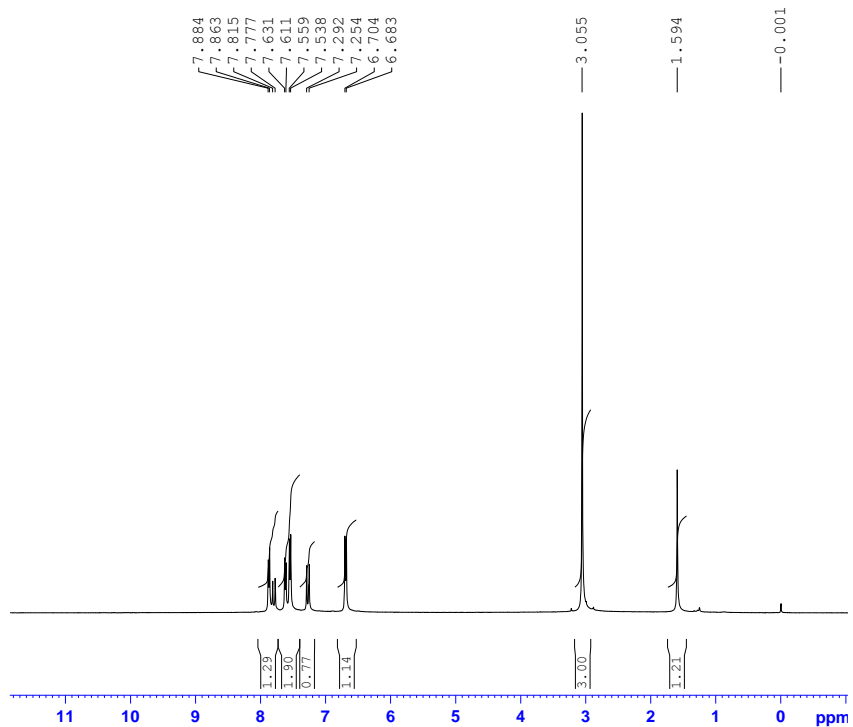
Figure 4.19: ¹H NMR spectrum of *(E)-1-(4-bromophenyl)-3-(4-(dimethylamino)phenyl)prop-2-en-1-one (CNBr).*
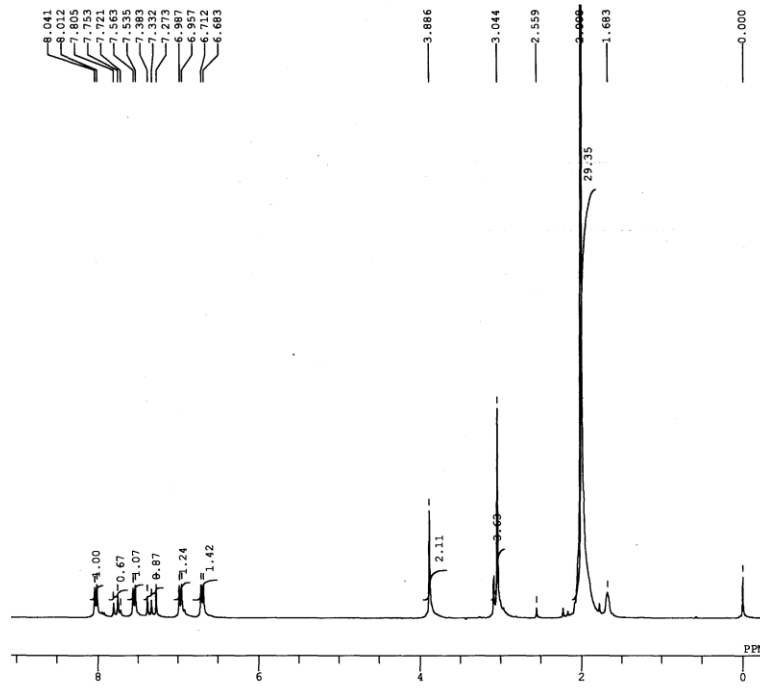
Figure 4.20: ¹H NMR spectrum of *(E)-3-(4-dimethyaminophenyl)-1-(4-methoxyphenyl)prop-2-en-1-one (PS 1).*
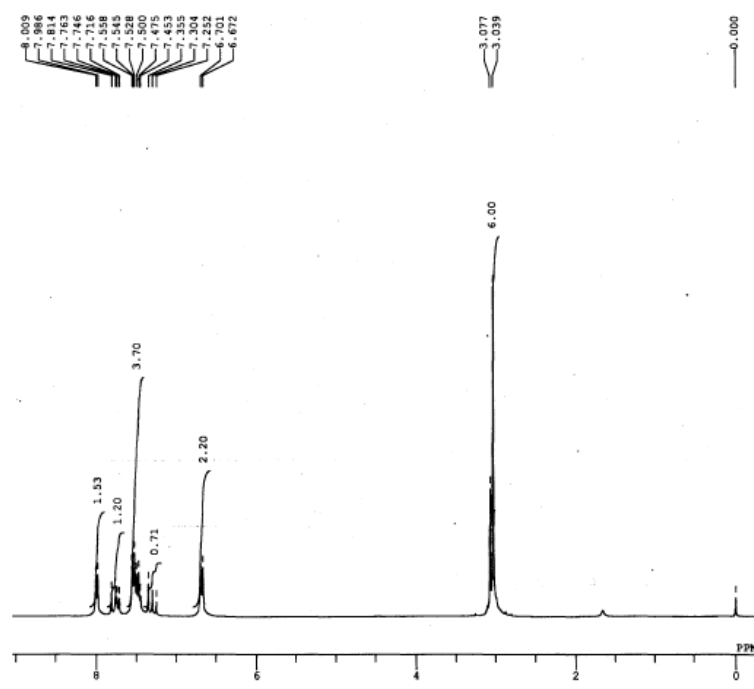
Figure 4.21: ¹H NMR spectrum of *(E)-3-(4-(dimethylaminophenyl)-1-phenyl prop-2-en-1-one* **(PS 2).**
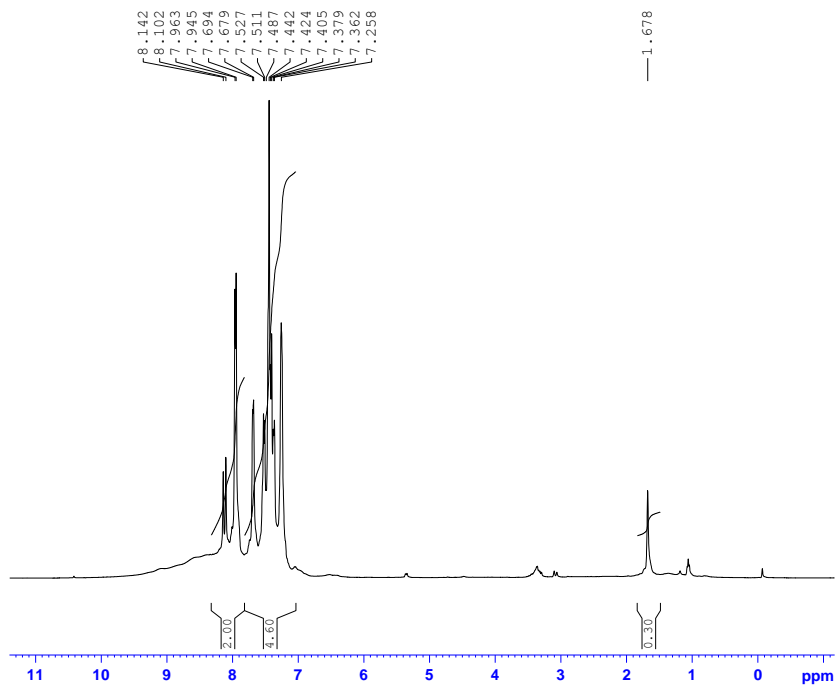
Figure 4.22:¹H NMR spectrum of *(E)-3-(2-chlorophenyl)-1-phenylprop-2-en-1one)* **(PS 9).**
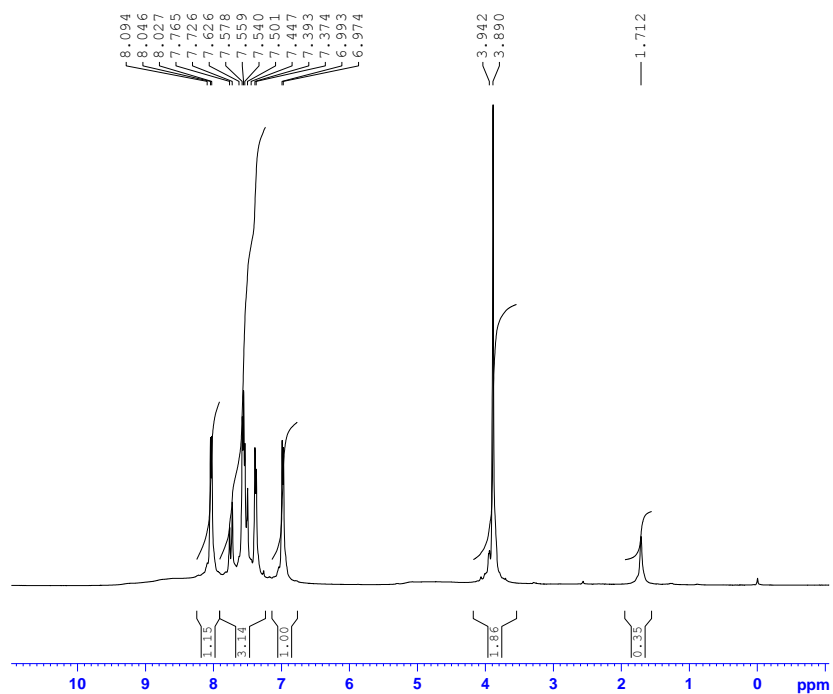
Figure 4.23:¹H NMR spectrum of *(E)-3-(4-chlorophenyl)-1-(4-methoxyphenyl)prop-2-en-1-one* (PS 10).
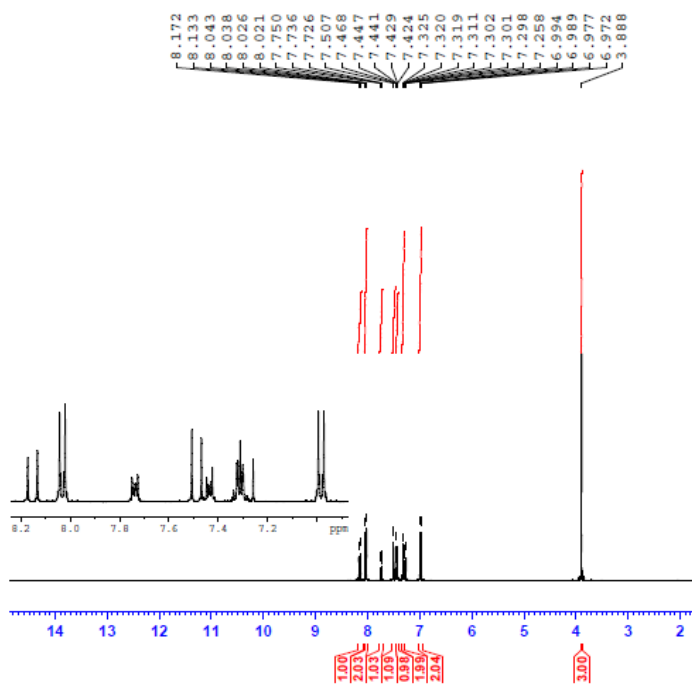
Figure 4.24:¹H NMR spectrum of *(E)-3-(2-chlorophenyl)-1-(4-methoxyphenyl)prop-2-en-1-one* (PS 16).
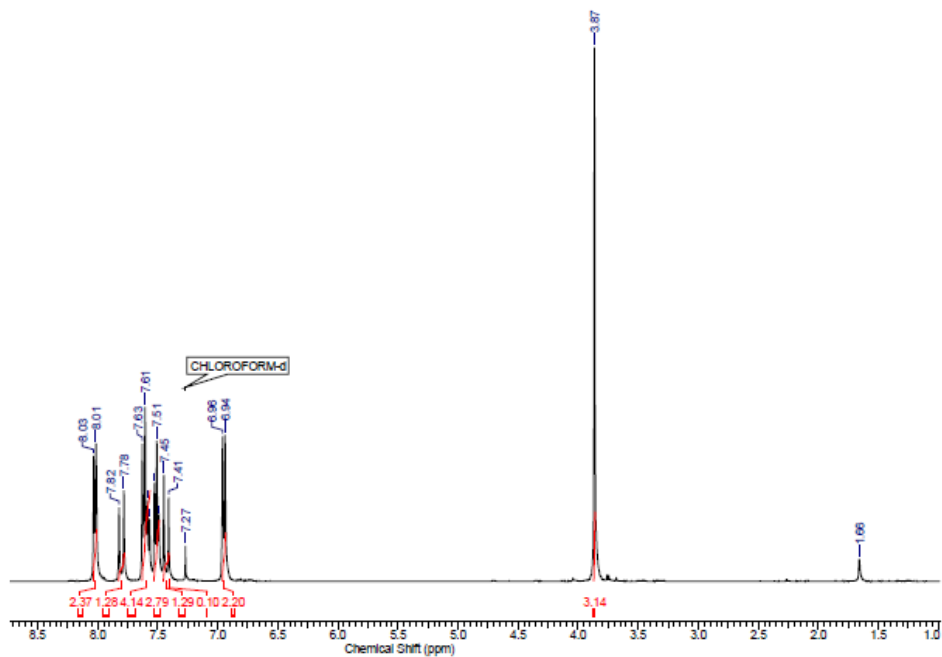
Figure 4.25:¹H NMR spectrum of *(E)-3-(4-methoxyphenyl)-1-phenylprop-2-en-1-one)* **(PS 27).**
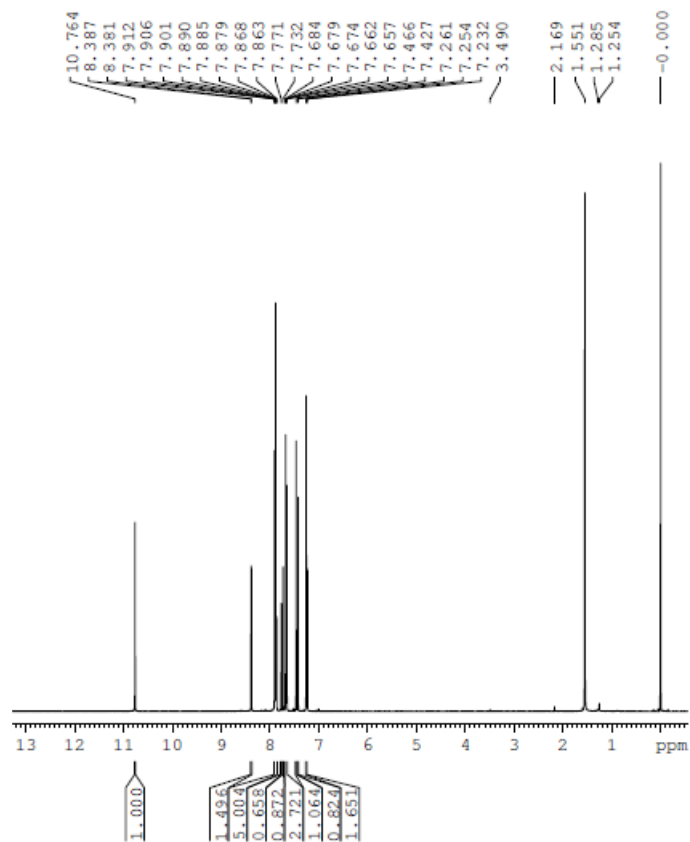
Figure 4.26:¹H NMR spectrum of *(E)-1-(4-bromophenyl)-3-(4-hydroxy-3-nitrophenyl) prop-2-en-1-one* **(OHNBr).**

13C NMR peaks labeled: 188.568, 156.384, 142.084, 136.551, 136.472, 132.050, 130.001, 127.519, 125.126, 121.889, 120.917, 77.254, 77.000, 76.746

240.0 220.0 200.0 180.0 160.0 140.0 120.0 100.0 80.0 60.0 40.0 20.0
: parts per Million : Carbon13
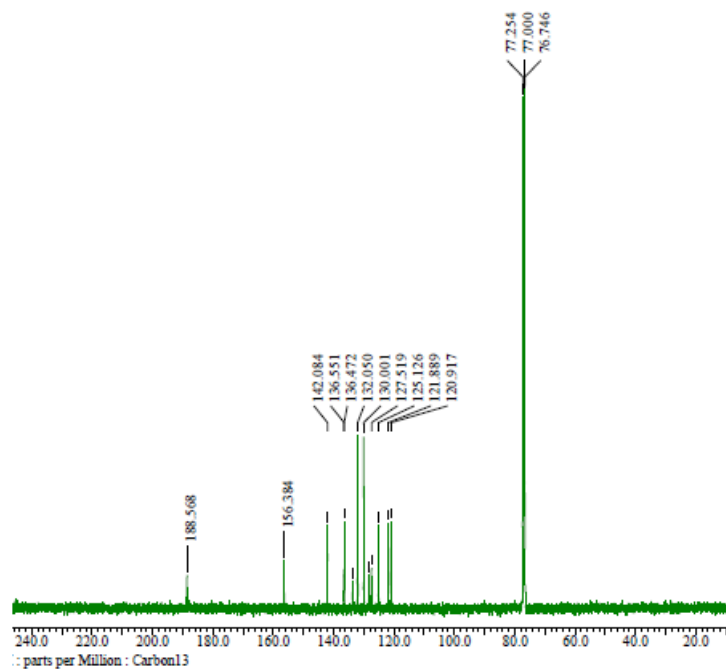
Figure 4.27:^{13}**C NMR spectrum of** *(E)-1-(4-bromophenyl)-3-(4-hydroxy-3-nitrophenyl) prop-2-en-1-one* **(OHNBr).**

ONC1

15 14 13 12 11 10 9 8 7 6 5 4 3 2 1 ppm
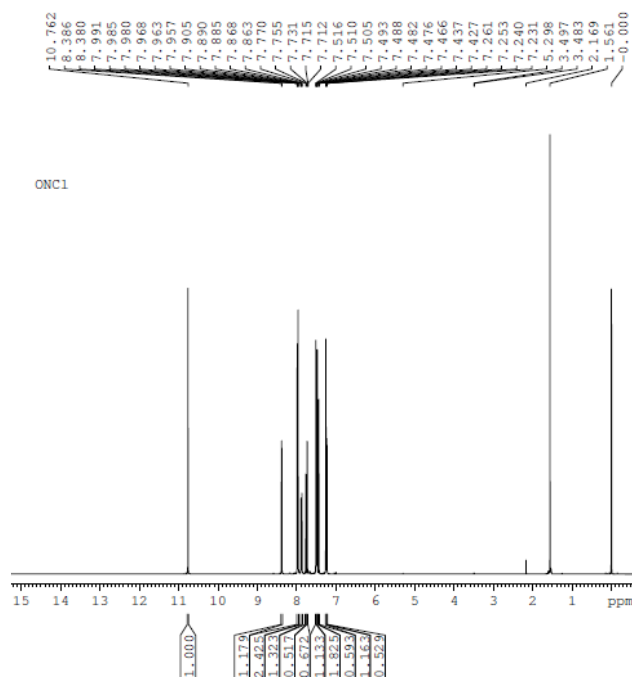
Figure 4.28:^{1}**H NMR spectrum of** *(E)-1-(4-chlorophenyl)-3-(4-hydroxy-3-nitrophenyl) prop-2-en-1-one* **(OHNCl).**
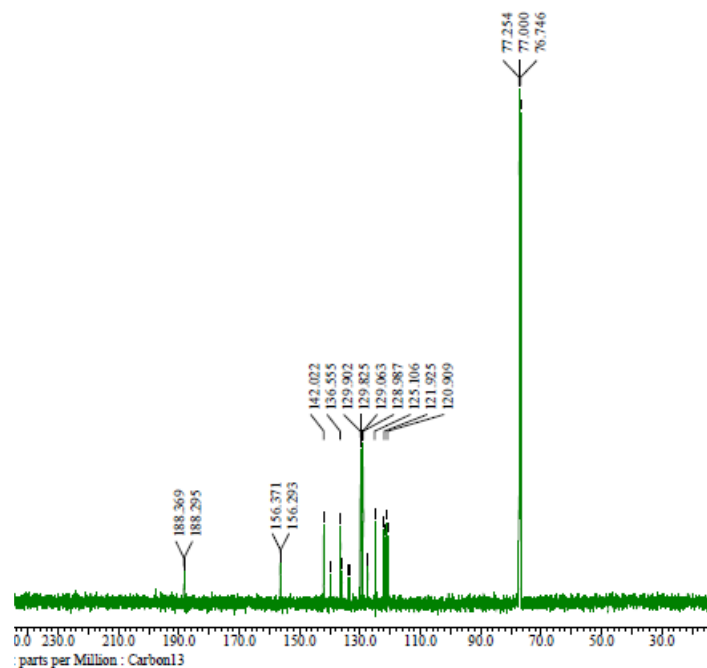
Figure 4.29: ^{13}**C NMR spectrum of** *(E)-1-(4-chlorophenyl)-3-(4-hydroxy-3-nitrophenyl) prop-2-en-1-one*
(OHNCl).
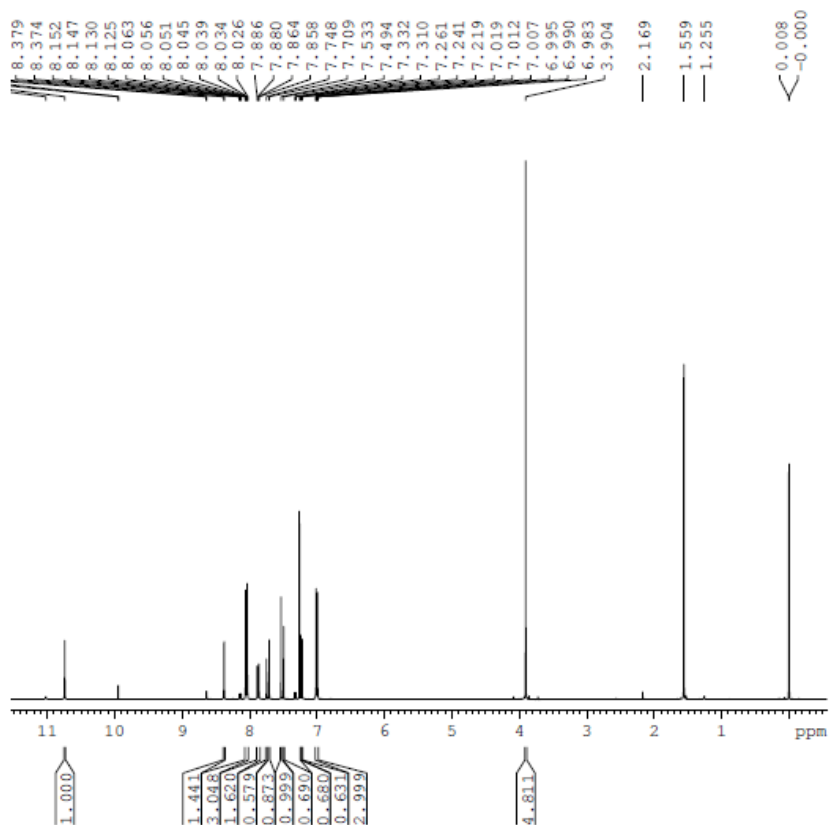
Figure 4.30: ^{1}**H NMR spectrum of** *(E)-3-(4-hydroxy-3-nitrophenyl)-1-(4-methoxyphenyl)prop-2-en-1-one*
(OHNMe).

74
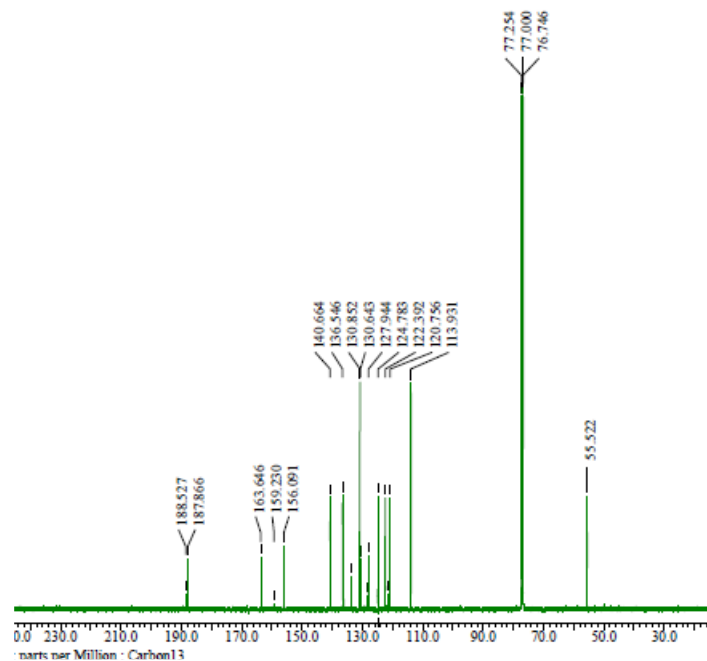
Figure 4.31:[13]**C NMR spectrum of** *(E)-3-(4-hydroxy-3-nitrophenyl)-1-(4-methoxyphenyl)prop-2-en-1-one* **(OHNMe).**
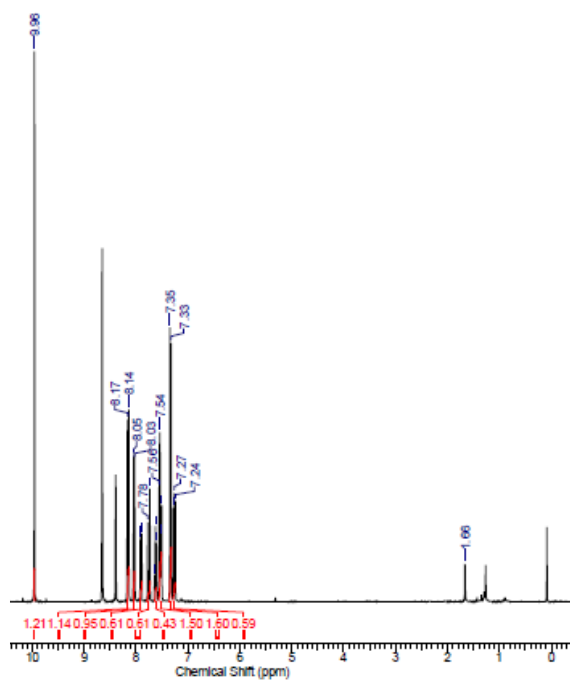
Figure 4.32:[1]**H NMR spectrum of** *(E)-3-(4-hydroxy-3-nitrophenyl)-1-phenylprop-2-en-1-one* **(OHNH).**
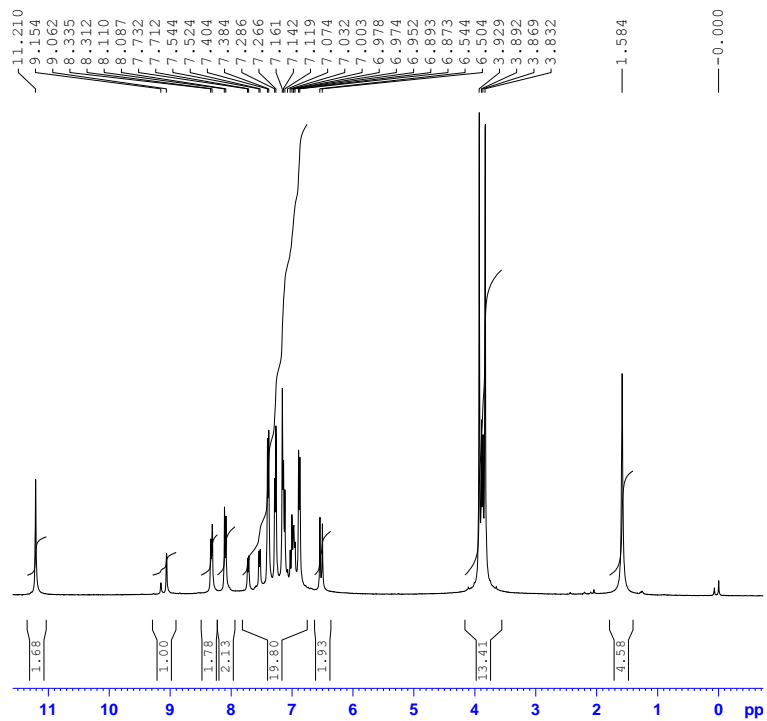
Figure 4.33:[1]**H NMR spectrum of** *(E)-1-((E)-1,3-bis(4-methoxyphenyl)allylidene)-2-(2,4-dinitrophenyl)hydrazine* **(PS 21).**
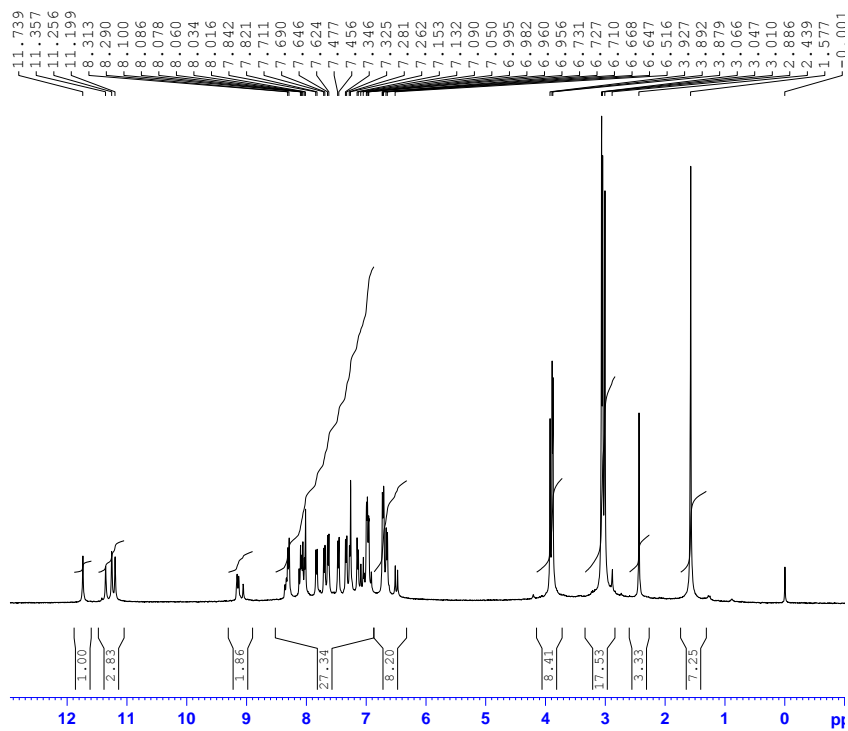
Figure 4.34:[1]**H NMR spectrum of** *4-((1E,3E)-3-(2-(2,4-dinitrophenyl)hydrazono)-3-(4-methoxyphenyl)prop-1-en-1-yl)-N,N dimethylaniline* **(PS 22).**
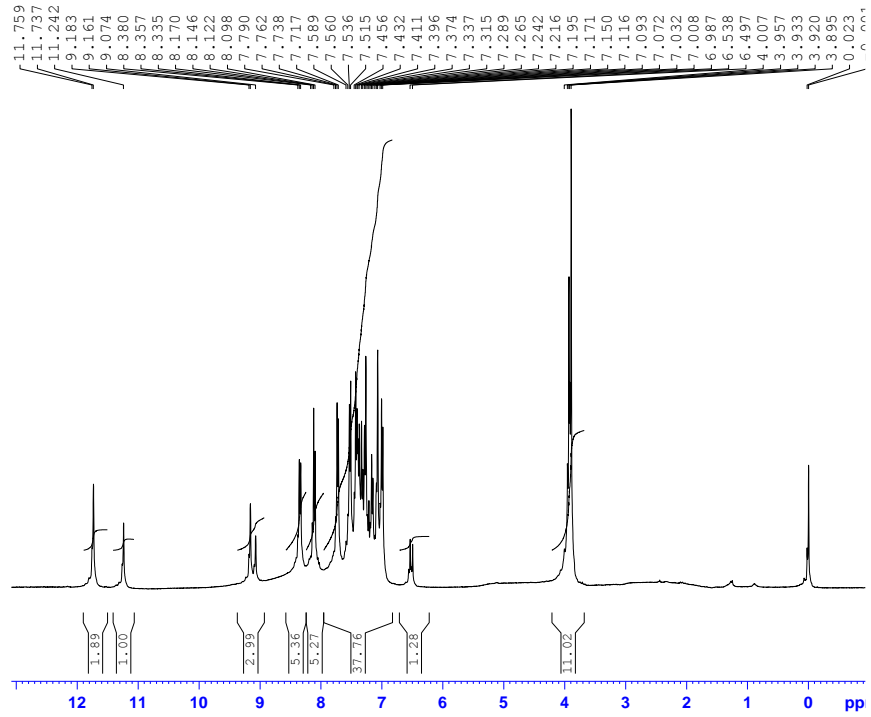
Figure 4.35: ^{1}H NMR spectrum of *(E)-1-((E)-3-(4-chlorophenyl)-1-(4-methoxyphenyl)allylidene)-2-(2,4 dinitrophenyl)hydrazine* **(PS 8).**
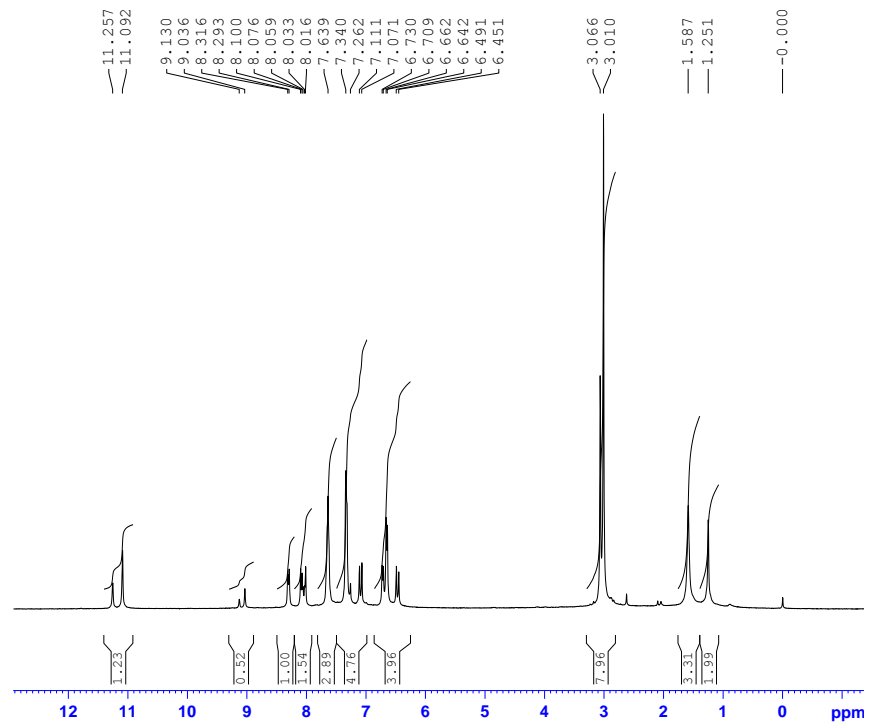
Figure 4.36: ^{1}H NMR spectrum of *4-((1E,3E)-3-(2-(2,4-dinitrophenyl)hydrazono)-3-phenylprop-1-en-1-yl)-N,N-dimethylaniline* **(PS 18).**
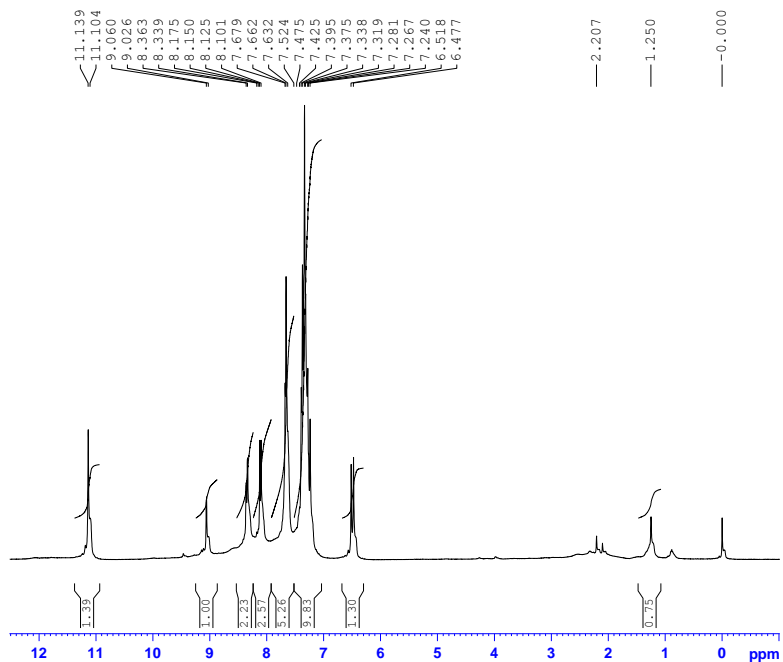
Figure 4.37:^{1}**H NMR spectrum of** *(E)-1-((E)-3-(4-chlorophenyl)-1-phenylallylidene)-2-(2,4-dinitrophenyl)hydrazine* **(PS 6).**

Open aperture z-scan data of chalcones:
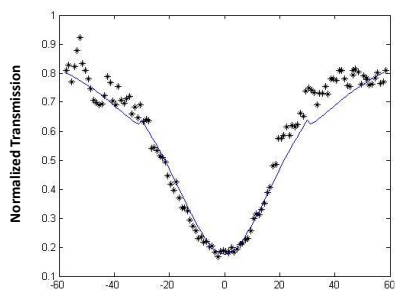
Figure 4.38: Open aperture z scan data of PS 1
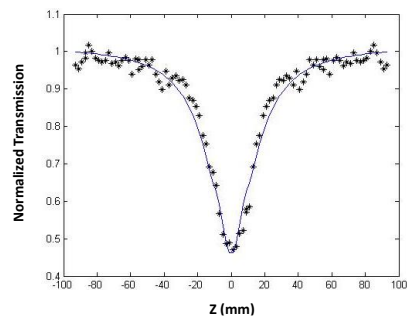
Figure 4.39: Open aperture z scan data of PS 16
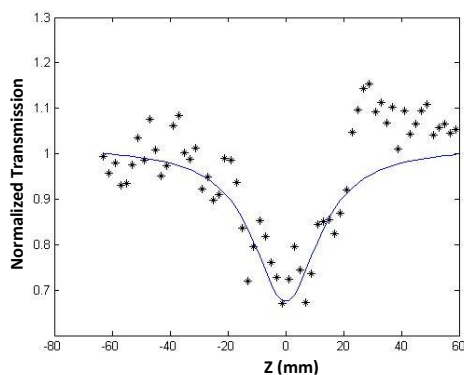
Figure 4.40: Open aperture z scan data of PS 5
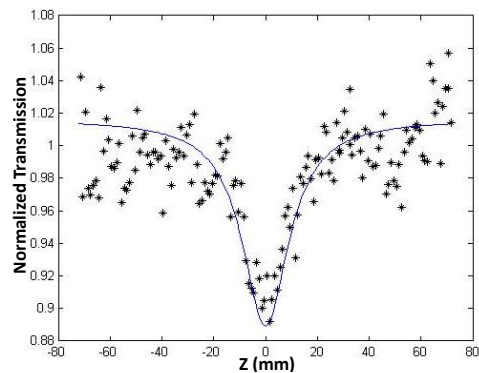
Figure 4.41: Open aperture z scan data of PS 2

78
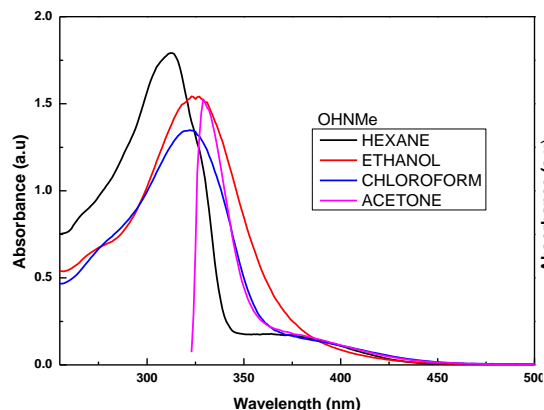
Figure 4.42: Absorption spectra of OHNMe in different solvent.
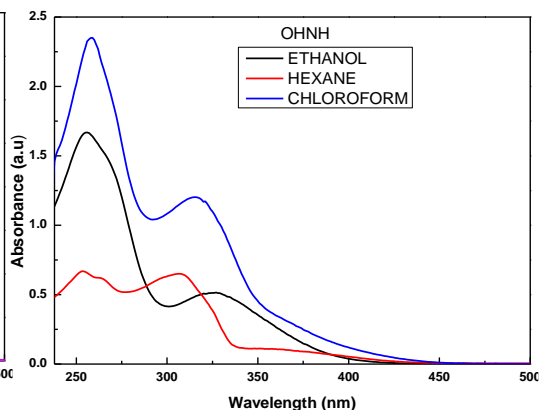
Figure 4.43: Absorption spectra of OHNH in different solvent.
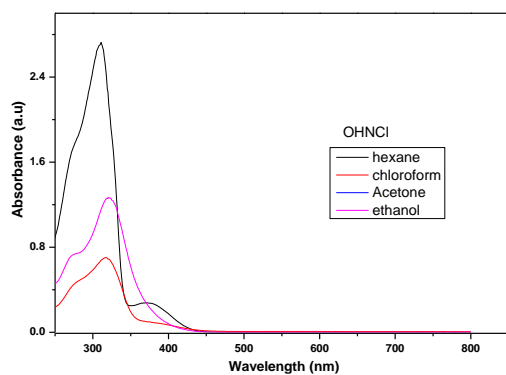
Figure 4.44: Absorption spectra of OHNCl in different solvent.
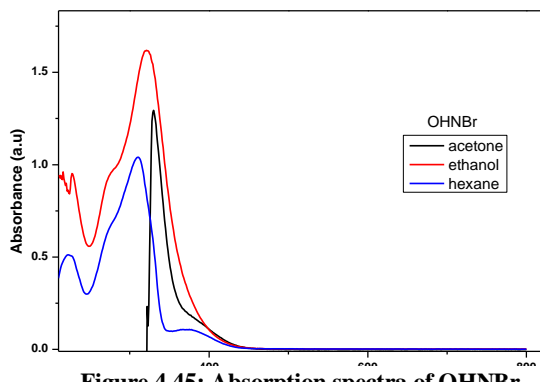
Figure 4.45: Absorption spectra of OHNBr in different solvent.
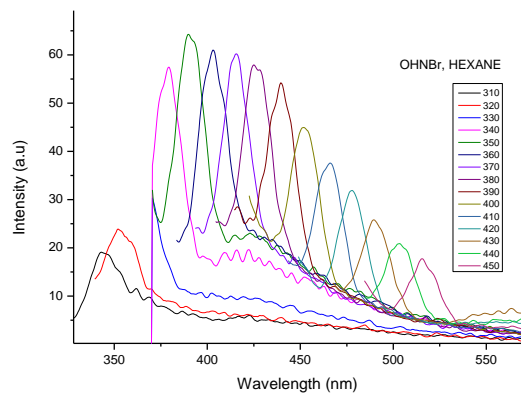
Figure 4.46: EDF of OHNBr in Hexane.
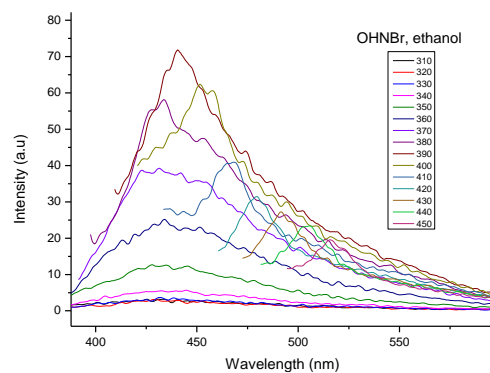
Figure 4.47: EDF of OHNBr in Ethanol.

79
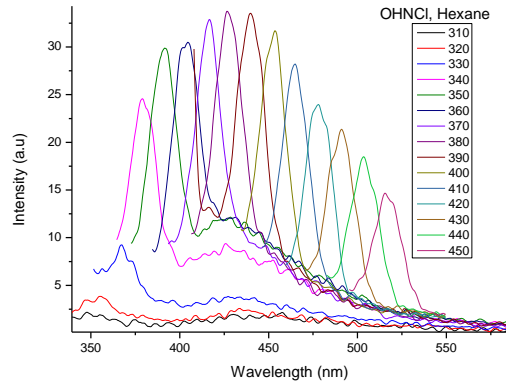
Figure 4.48: EDF of OHNCl in Hexane.
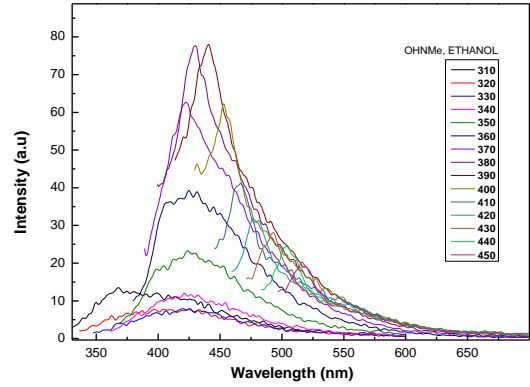
Figure 4.49: EDF of OHNMe in Ethanol.
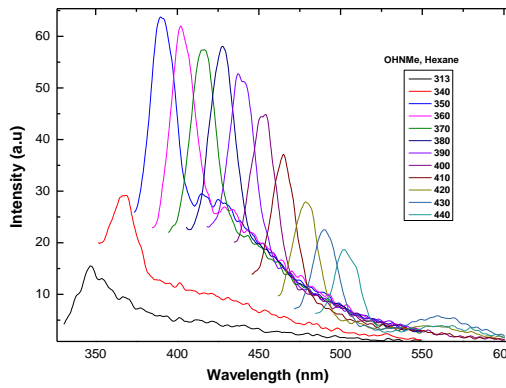
Figure 4.50: EDF of OHNMe in Hexane
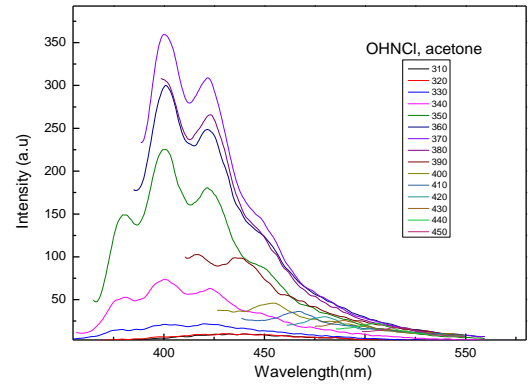
Figure 4.51: EDF of OHNCl in Acetone.
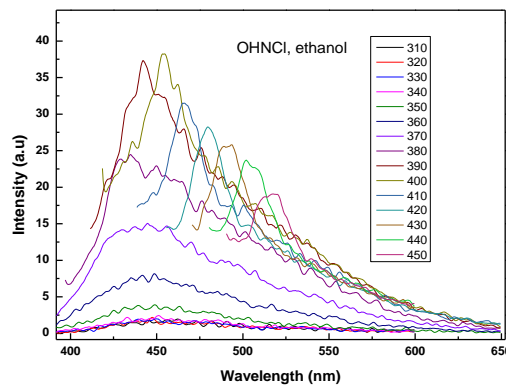
Figure 4.52: EDF of OHNCl in Ethanol.
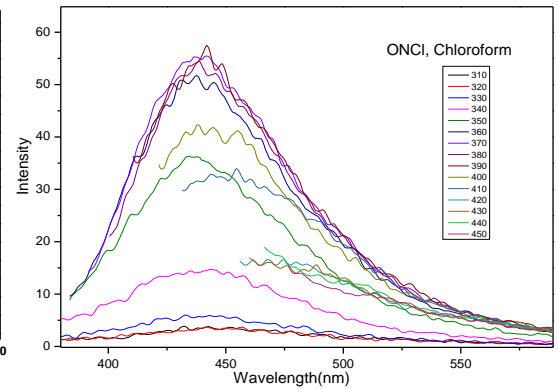
Figure 4.53: EDF of OHNCl in Chloroform.
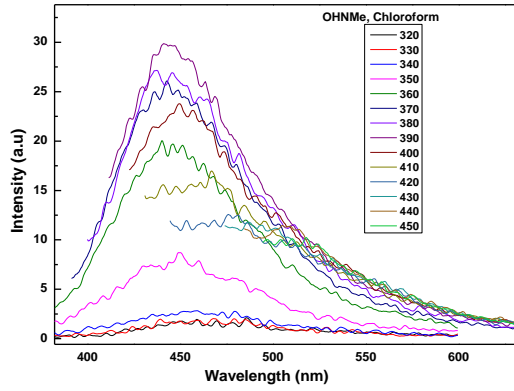
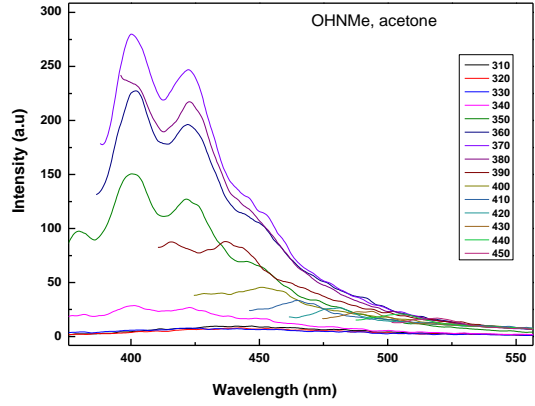**Figure 4.54: EDF of OHNMe in Chloroform.**

Figure 4.55: EDF of OHNMe in Acetone.

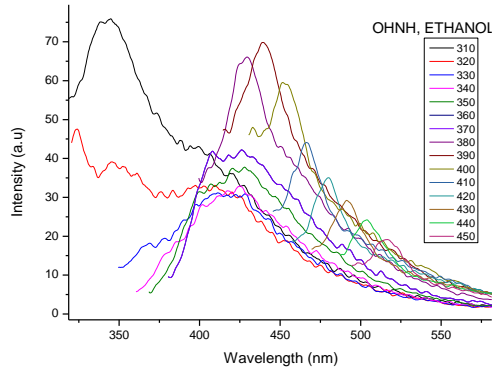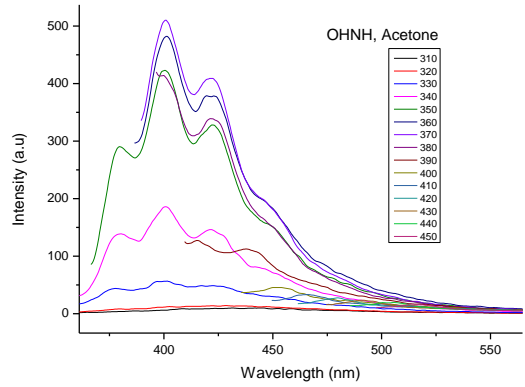**Figure 4.56: EDF of OHNH in Ethanol.**

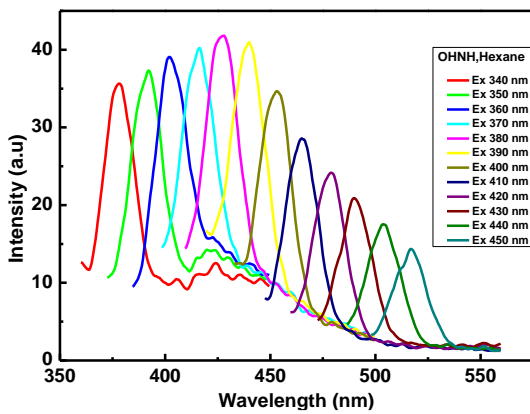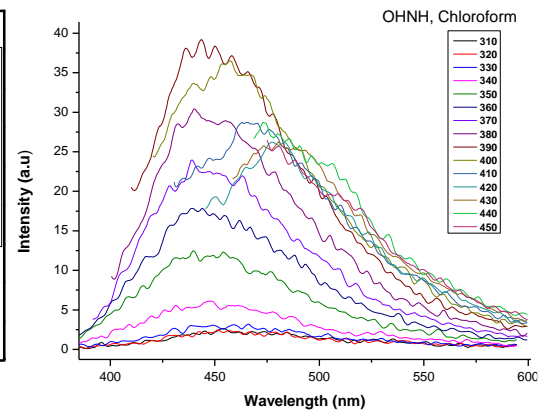**Figure 4.57: EDF of OHNH in Acetone.**

Figure4.58: EDF of OHNH in Hexane

Figure 4.59: EDF of OHNH in Chloroform

81